



1 **Real-world observations of ultrafine particles and reduced nitrogen in**
2 **commercial cooking organic aerosol emissions**

3 Sunhye Kim¹, Jo Machesky², Drew R. Gentner², Albert A. Presto¹

4 ¹ Department of Mechanical Engineering and Center for Atmospheric Particle Studies, Carnegie
5 Mellon University, Pittsburgh, Pennsylvania, United States

6
7 ² Department of Chemical & Environmental Engineering, Yale University, New Haven,
8 Connecticut 06511, United States

9
10 Correspondence: Albert A. Presto (apresto@andrew.cmu.edu)

11

12 **Abstract**

13 Cooking is an important but understudied source of urban anthropogenic fine particulate matter
14 (PM_{2.5}). Using a mobile laboratory, we measured PM size and composition in urban restaurant
15 plumes. Size distribution measurements indicate that restaurants are a source of urban ultrafine
16 particles (UFPs, particles <100 nm diameter), with a mode diameter <50 nm across sampled
17 restaurants and particle number concentrations (PNC, a proxy for UFPs) that were substantially
18 elevated relative to the urban background. The majority of observed PM was organic aerosol
19 (OA) by mass. Aerosol mass spectra show that while emissions from most restaurants were
20 similar, there were key mass spectral differences. All restaurants emit OA at m/z 41, 43, and 55,
21 though the composition (e.g., the ratio of oxygenated to reduced ions at specific m/z) varied
22 across locations. All restaurant emissions included reduced nitrogen species detected as C_xH_yN⁺
23 fragments, making up ~15% of OA mass measured in plumes, with reduced molecular
24 functionalities (e.g., amines, imides) that were often accompanied by oxygen-containing
25 functional groups. The largest reduced nitrogen emissions were observed from a commercial



26 bread bakery (i.e., 30-50% of OA mass), highlighting the marked differences between restaurants
27 and their importance for emissions of both urban UFPs and reduced nitrogen.

28

29 **Introduction**

30 Concentrations of most air pollutants, including fine particulate matter (PM_{2.5}) and
31 ultrafine particles (UFPs; particles with diameter <100 nm), are typically higher in urban areas
32 compared to rural or suburban areas (Cheng et al., 2019; Chow et al., 2006; Lenschow et al.,
33 2001; Louie et al., 2005; Renzi et al., 2021; Wang et al., 2020). Elevated urban concentrations
34 lead to higher human exposure, and in turn, contribute to the health impacts of air pollution.
35 PM_{2.5} exposures are associated with cardiovascular disease, lung cancer, and asthma and
36 contribute to up to 100,000 deaths annually in the US (Castillo et al., 2021). Although health
37 effects of UFP exposure are less extensively studied compared to PM_{2.5} (Schraufnagel, 2020) and
38 are an area of ongoing research, there is growing evidence that UFPs can enhance acute health
39 effects because of their small size and high surface area (Ali et al., 2022; Ibald-Mulli et al., 2002;
40 Kwon et al., 2020).

41 The PM_{2.5} and UFP concentration enhancements in many urban areas are strongly
42 influenced by anthropogenic emissions (Apte et al., 2017; Li et al., 2018; Mohr et al., 2011; Saha
43 et al., 2019). Among a wide variety of contributing sources, two notable urban sources are
44 mobile sources (e.g., motor vehicles) and cooking. These two sources contribute to urban
45 enhancements relative to the non-urban areas and to intra-urban spatial variations in PM_{2.5} and
46 UFP concentrations (Klompaker et al., 2015). In prior work, mobile sources and cooking
47 emissions have led to neighborhood-scale enhancements of ~0.5-1 µg m⁻³ of PM_{2.5} in North



48 American cities and a factor of two enhancement in UFPs (Rose Eilenberg et al., 2020; Song et
49 al., 2021b).

50 Motor vehicle emissions are well studied and have seen dramatic reductions as a result of
51 effective regulations on PM emissions across Europe and the US (Font et al., 2019; Keuken et
52 al., 2012). In contrast, there has been less attention to cooking sources as contributors of PM and
53 UFP emissions. As such, there have been fewer direct measurements and regulations dedicated
54 to cooking-related emissions, including everyday sources such as restaurants and home kitchens.
55 For comparison, two studies conducted in Pasadena, California revealed that organic PM_{2.5}
56 attributed to cooking decreased from approximately 2.4 µg/m³ to 1.2 µg/m³ between 1982 and
57 2010, while the contribution from traffic sources dropped from about 6.8 µg/m³ to 0.82 µg/m³
58 (Hayes et al., 2013; Schauer et al., 1996). This means that while total PM_{2.5} and vehicular-related
59 primary PM_{2.5} have decreased, the fraction of urban PM_{2.5} attributed to cooking has increased.

60 Aerosol mass spectrometry (AMS) measurements worldwide further indicate the
61 importance of cooking PM. Factor analysis of AMS using PMF (Positive Matrix Factorization)
62 data routinely identifies a Cooking Organic Aerosol (COA) factor that accounts for 6 - 25% of
63 the total organic aerosol (OA) in urban environments. Specifically, a measurement study in
64 Athens and Patras, Greece, showed that the COA contribution increased to 75% of organic PM₁
65 during mealtime in Patras (Florou et al., 2017). While the COA factor is routinely identified,
66 there can be significant variation in its composition from city to city (Bozzetti et al., 2017;
67 Crippa, El Haddad, et al., 2013; R. Hu et al., 2021; X.-F. Huang et al., 2010; Lee et al., 2015;
68 N. Pandis et al., 2016; Rogge et al., 1991a; Sun et al., 2012).

69 Many potential factors could produce variability in the composition and size distribution
70 of cooking PM. While the UFPs from cooking can contribute to ~ 80% of the total particle



71 number concentrations indoors (Wan et al., 2011), there are a lot of factors—such as indoor-
72 outdoor air exchange rates (Wallace et al., 2004) and types of cooking oils used (Torkmahalleh
73 et al., 2012)—that can determine the size distribution of particles as well as the $PM_{2.5}$
74 concentrations from cooking activities. There is some evidence that the chemical composition of
75 cooking emissions may vary with the cooking style and the food cooked (Omelekhina et al.,
76 2020; Reyes-Villegas et al., 2018a; Takhar et al., 2019). For example, the cooking temperature,
77 ingredients, and methods used can alter chemical pathways that lead to the generation of
78 nitrogen-containing functional groups, including amides, within COA (Ditto et al., 2022).
79 Multiple studies found that nitrogen composition has been observed while charbroiling (Rogge et
80 al., 1991a) or deep-frying hamburgers (Reyes-Villegas et al., 2018b; Rogge et al., 1991a).
81 Masoud et al., (2022) found that nitrogen-containing compounds contributed 12-19% of the
82 signal measured by a chemical ionization mass spectrometer for emissions from typical in-home
83 cooking. Overall, this variability across diverse cooking styles and conditions is relevant but
84 poorly understood. This implies a significant need for real-world measurements to characterize
85 and understand particle size and composition of cooking emissions in urban environments.

86 This study aimed to characterize cooking emissions from real-world restaurant sources in
87 the US. We used a mobile laboratory to measure cooking emissions from nine restaurants in
88 Pittsburgh, PA and Baltimore, MD. Four of these restaurants were visited twice, making for a
89 total of thirteen cooking sites. Several analytical instruments, including an AMS and FMPS (Fast
90 Mobility Particle Sizer), were used at each site for online measurements, with supplemental PM
91 collection on Teflon filters for offline analysis. The measurements are used to examine variations
92 in UFP concentrations and cooking OA composition measured outside of restaurants with a



93 focus on contributions from reduced nitrogen components across restaurant sites visited during
 94 the field campaign.

95

96 **2. Methods**

97 *2.1 Measurement locations*

98 **Table 1.** Summary of restaurant locations and concentration enhancements measured in the
 99 cooking emission plumes. Several restaurants were sampled on two separate days, as indicated
 100 by the number following the restaurant identifier. AMS high-resolution analysis of mean OA
 101 enhancement (CE=1), mean BC enhancement from aethalometer, Mode D_p (nm), mean f_{41} (the
 102 fraction of mass-to-charge ratio at 41 to the total organic mass signal), f_{43} , and f_{55} .

	City	Mean Δ OA ($\mu\text{g}/\text{m}^3$)	Mean Δ BC ($\mu\text{g}/\text{m}^3$)	Mode D_p (nm)	f_{41}	f_{43}	f_{55}
Island Cuisine	Pittsburgh	65	0.83	17	0.068	0.054	0.094
Pizza	Pittsburgh	100	3.2	29	0.070	0.058	0.096
BBQ	Baltimore	1.2	0.38	11	0.061	0.058	0.070
Café	Baltimore	2.3	0.35	8.1	0.044	0.082	0.043
Beef	Baltimore	15	4.2	11	0.082	0.074	0.10
Diner 1	Pittsburgh	77	1.4	11	0.065	0.044	0.078
Diner 2	Pittsburgh	84	2.0	11	0.078	0.054	0.092
Bakery 1	Baltimore	12	0.091	8.1	0.011	0.023	0.003
Bakery 2	Baltimore	4.6	0.41	8.1	0.053	0.048	0.003
Fast Food 1	Baltimore	1.7	1.4	29	0.030	0.064	0.024
Fast Food 2	Baltimore	3.8	0.36	11	0.053	0.048	0.013
Bar/Restaurant 1	Baltimore	69	2.4	11	0.086	0.066	0.10
Bar/Restaurant 2	Baltimore	140	5.0	26	0.076	0.076	0.12

103

104 Field samples were collected from 13 visits to 9 urban cooking sites in Pittsburgh and
 105 Baltimore during July and August 2019 (Table 1). At each location, we parked a mobile
 106 laboratory near the restaurant's exhaust plume (SI Fig. 1). The selected restaurants represent a
 107 mix of accessible locations with visible emission plumes or exhaust vents. The sampling inlet on
 108 the mobile laboratory was typically within a few meters of the exhaust vent. However, this
 109 distance varied due to several uncontrollable external factors, such as the availability of parking



110 and the height of the restaurants' exhaust vents. As a result, the measured emission plumes went
111 through varying degrees of dilution before reaching our sampling inlet.

112 Several of the restaurants were sampled on multiple visits to examine day-to-day
113 variations in emissions. These variations could be due to differences in activity (e.g., how many
114 customers ordered food), the type of food ordered, and differences in dilution conditions. Each
115 visit to a restaurant site lasted approximately 30-60 minutes. The sampling periods targeted
116 expected times for lunch (~11 am – 1 pm) and dinner (~6 – 8 pm).

117

118 *2.2 Mobile laboratory and measurements*

119 Instruments were loaded into a gasoline-powered mobile laboratory. At each location, we
120 oriented the mobile laboratory so that the vehicle exhaust was located downwind of the sample
121 inlet to minimize self-contamination from the vehicle exhaust.

122 We use total particle number concentration (PNC) as our proxy for UFPs. Particle
123 number counts were measured by a MAGIC™ water CPC (Moderated Aerosol Growth with
124 Internal water Cycling Condensation Particle Counter, Aerosol Devices Inc, Model
125 MAGIC200P). MAGIC CPC uses water condensation to enlarge particles through a 3-
126 temperature stage growth tube. The enlarged particles are counted with a laser sensor up to
127 400,000 particles cm^{-3} with a particle size range between 5 nm and 2.5 μm in diameter (Hering et
128 al., 2019). Saha et al., (2019) previously observed that the MAGIC CPC undercounts relative to a
129 butanol CPC. Thus, the raw CPC output was adjusted using a correction factor determined from
130 the co-location of the MAGIC CPC with a TSI 3772 butanol CPC.

131 Particle size distributions and total number concentrations were measured with FMPS
132 (Fast Mobility Particle Sizer, TSI Inc, Model 3091) for particles with diameters from 6.04 nm to



133 523.3 nm. The FMPS reported systematically lower particle counts than the MAGIC CPC (factor
134 of 3.5, SI Section 2 and Fig. S2). FMPS data were utilized in lieu of the CPC data due to high
135 particle number concentrations in restaurant plumes that exceeded the upper counting limit of the
136 CPC (400,000 particles cm^{-3}), resulting in error flags. To ensure consistency with the MAGIC
137 CPC, all FMPS data were corrected by integrating the FMPS size distribution, which was scaled
138 by the FMPS:CPC ratio.

139 A High-Resolution AMS (HR-AMS, Aerodyne), which measures non-refractory particles
140 with a diameter less than 1 μm (NR- PM_{10}), was used to identify mass spectra of PM components
141 (Organics, NH_4^+ , NO_3^- , SO_4^{2-} , and Cl^-) in real-time. Squirrel (SeQUential Igor data RetTriEvaL)
142 toolkit 1.62G and Pika (Peak Integration by Key Analysis) toolkit 1.22G in Igor Pro
143 (Wavemetrics, Lake Oswego) were used for the HR-AMS data analysis. For the baseline and
144 peak fitting correction procedures of the HR-AMS data, the high-resolution range of m/z (mass-
145 to-charge ratios) 12 to 140 was selected. All AMS analysis presented here assumes a collection
146 efficiency (CE) of one.

147 An aethalometer (Magee Scientific, Model AE33), CO analyzer (Teledyne API T300),
148 and CO_2 analyzer (LiCor LI-820, Biosciences) measured black carbon (BC), CO, and CO_2
149 concentration, respectively.

150 $\text{PM}_{2.5}$ samples were collected at ~ 70 L/min on 47 mm PTFE membrane filters (47 mm,
151 2.0 μm pores, Tisch Scientific) through a separate inlet mounted close to the online
152 instrumentation inlet outfitted with a cyclone (2.5 μm cut point with a flow rate of 92 LPM,
153 URG-2000-30EH, URG cyclone). At each restaurant site where plumes were observed via AMS,
154 a filter sample was collected for at least 30 minutes and Table S3 shows details for each filter
155 sample. Filter samples were transported on ice packs from the mobile lab and kept in sample



156 storage freezers. Additional filter collection details can be found in the Supporting Information.
157 All samples were analyzed via liquid chromatography (LC) using an Agilent Infinity LC and an
158 Agilent Poroshell 120 SB-Aq reverse-phase column (2.1×50 mm, 2.7 μm particle size). The LC
159 was coupled to an electrospray ionization (ESI) source, operated in positive and negative modes
160 for each sample, and connected to a high-resolution mass spectrometer (Agilent 6550 Q-TOF).
161 These instruments were operated following previously described methods (Ditto et al., 2018,
162 2020).

163 Selected samples showing unique AMS spectra with nitrogen-containing compounds
164 underwent further analysis via MS/MS (tandem mass spectrometry) with the objective of
165 identifying the distribution of functional groups within the reduced nitrogen species that were
166 observed via LC-TOF, similar to prior work (Ditto et al., 2020, 2022). LC-TOF mode data
167 processing and QC/QA have previously been described (Ditto et al., 2018), and details of
168 compound selection for MS/MS analysis in this study can be found in the Supporting
169 Information (Section S3). MS/MS spectra analysis used SIRIUS with CSI:FingerID for
170 molecular structure prediction (Dührkop et al., 2015, 2019), and the APRL Substructure Search
171 Program was used for functional group identification from the predicted SMILES formula for
172 atmospherically-relevant groups (Ruggeri & Takahama, 2016). Further details on LC-MS/MS
173 analysis, processing, and associated limitations of ESI and MS/MS spectra analysis can be found
174 in Ditto et al., (2020), with brief comments on relevant SIRIUS updates in the Supporting
175 Information (Section S3).

176

177

178



179 **3. Results and Discussion**

180 *3.1 Typical measurements of restaurant emission*

181 Figure 1 demonstrates observations collected during a typical sampling day via the
182 mobile lab in Baltimore. On this day, the mobile laboratory was initially (~15:36 – 16:49 EDT)
183 parked in an urban park, here noted as background. Sampling was then conducted on-road,
184 driving on various streets in urban Baltimore, from 16:49 to 18:20. At 18:20; the mobile
185 laboratory was parked outside a restaurant (Bar/Restaurant 2).

186 The data in Figure 1 exemplify clear variations in pollutant concentrations between the
187 background, on-road, and restaurant portions of sampling. In general, concentrations were the
188 lowest and least variable in urban background locations and the highest and most variable for the
189 restaurant sampling periods.

190 Nearby vehicles likely impacted the measured concentrations during the on-road
191 sampling period, thus differentiating it from the background period, where direct observations of
192 on-road emissions were minimal. Concentrations of CO, CO₂ (Fig. 1a), organic aerosol (OA),
193 black carbon (BC, Fig. 1b), and particle number (Fig. 1d) were all elevated in the on-road
194 samples compared to the urban background. Δ OA and Δ BC were calculated by subtracting the
195 background concentration from the measured OA or BC mass concentration. The background
196 concentration is defined as the 5th percentile of data collected on each sampling day (listed in
197 Table S1).

198 The mean organic aerosol concentrations are 5.8 $\mu\text{g}/\text{m}^3$ (Δ OA: 2.46 $\mu\text{g}/\text{m}^3$) during on-
199 road sampling versus 4.2 $\mu\text{g}/\text{m}^3$ (Δ OA: 0.85 $\mu\text{g}/\text{m}^3$) in the urban background (Fig. 1b). Similarly,
200 the BC concentration was 0.5 $\mu\text{g}/\text{m}^3$ higher on-road than in the urban background, and PNC was
201 approximately a factor of three higher on-road than in the urban background. These



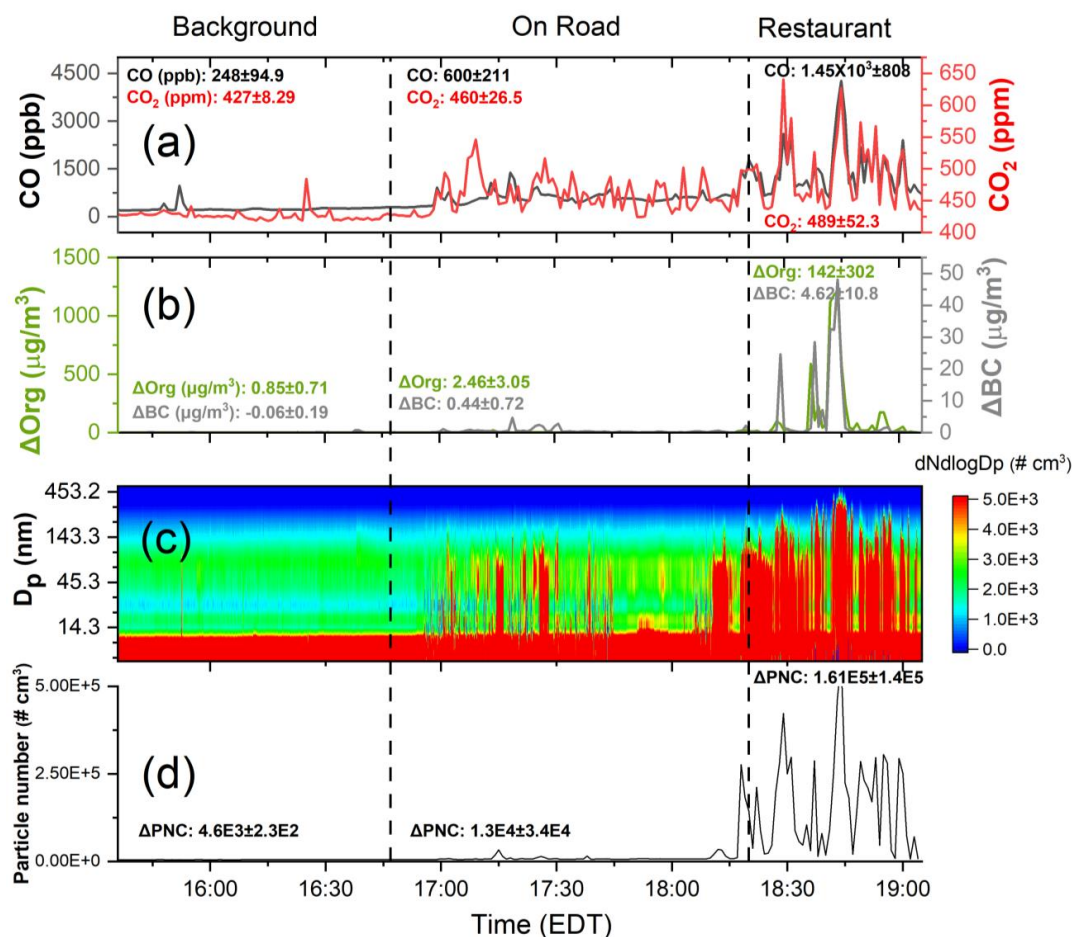
202 enhancements in organic aerosol, black carbon, and PNC are broadly consistent with
203 enhancements with those seen in high-traffic areas by our previous sampling in Pittsburgh and
204 Oakland (Saha et al., 2020; Shah et al., 2018).

205 In addition to the overall increase in pollutant concentrations on-road, there are
206 occasional, coincident spikes in CO, BC, OA, and PNC during the on-road sampling. The
207 particle size distribution also changes during these spikes (Fig. 1c), with higher concentrations of
208 particles in the 20-100 nm size range. These are likely plumes from high-emitting vehicles,
209 potentially diesel trucks and buses (Dallmann et al., 2013; Tan et al., 2016).

210 The highest and most variable concentrations are observed in the restaurant plume. In this
211 near-source environment, organic aerosol concentrations averaged $146 \mu\text{g}/\text{m}^3$. This is 35 times
212 higher than the urban OA background. Particle number counts were also 35 times higher in
213 concentration than background levels. CO, CO₂, and BC enhancements were also observed
214 when the mobile lab was parked near the restaurant. The enhancement of CO was 5.9 times the
215 background, CO₂ and BC were 1.15 and 5.42 times higher, respectively.

216 During the restaurant sampling period, there are several clear and concurrent spikes in
217 OA (Fig. 1b) and particle number count (Fig. 1d). These seem to be associated with specific
218 events, such as preparing a customer's new order (restaurant kitchens had varying activity levels
219 during the sampling periods). The size distributions in Figure 1c show that these emissions span
220 a wide range in particle size, from <10 nm up to a few hundred nm, demonstrating that
221 restaurants may be a source of urban ultrafine particles.

222



223

224

225 **Figure 1.** Urban background, on-road, and restaurant plumes observed during a typical sampling

226 day (Bar/Restaurant 2) in Baltimore, showing: (a) CO and CO₂, (b) background corrected

227 organic aerosol (OA) and black carbon (BC) concentrations, (c) particle size distribution from

228 FMPS, and (d) background-corrected total particle number concentrations. All concentrations

229 were significantly higher and more variable in restaurant emissions plume than in the urban

230 background or on-road period. Numbers in (a), (b), and (d) indicate the mean ± standard

231 deviation for each sampling period.

232

233 While average BC concentrations were about a factor of five higher than background

234 during the restaurant sampling period, BC seems to be a relatively smaller component of PM

235 emissions from the restaurant. The OA/BC ratio in the urban background and on-road sampling



236 periods was ~ 4 . In the restaurant plume, the mean OA/BC ratio was 28. Despite occasional
237 periods of very high BC concentrations reaching up to $58 \mu\text{g}/\text{m}^3$, the OA/BC ratio during the
238 spike was 230 (Fig. S3). Other PM components (e.g., sulfate and nitrate) show no discernable
239 enhancement during the restaurant sampling period (Fig. S4). This indicates that the PM
240 emissions from the restaurant were dominated by organic aerosol.

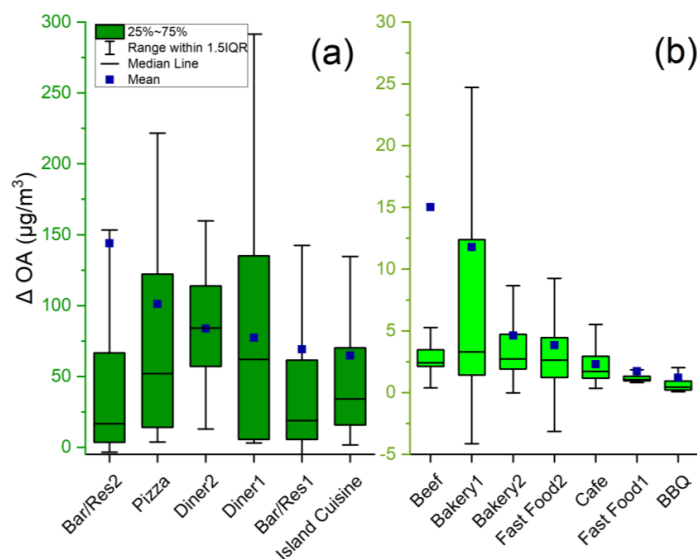
241 We also observed elevated concentrations of CO and CO₂ in the restaurant exhaust. We
242 do not have information about each restaurant's cooking practices or fuels (i.e., whether the
243 restaurants used natural gas or electricity). Jung & Su (2020) showed that food cooking emits
244 CO, so the CO spikes observed here may also be from the food rather than fuel combustion.
245 Other recent measurements in Pittsburgh by (Song et al., 2021a) also showed enhancements in
246 CO during mealtimes in a restaurant-rich area.

247

248 *3.2 Summary of organic aerosol enhancements at restaurant sites*

249 Enhancements in OA as a result of emissions from restaurants were similarly observed
250 across all other sampling sites that we visited. Figure 2 is a box-plot visualization of the OA
251 enhancement (ΔOA) for each restaurant visit. The data are split into two main groups for visual
252 clarity: high concentration (mean $\Delta\text{OA} > 50 \mu\text{g m}^{-3}$, Fig. 2a) and low concentration (mean ΔOA
253 $< 30 \mu\text{g m}^{-3}$, Fig. 2b).

254



255

256 **Figure 2.** Organic aerosol enhancement (ΔOA) at each restaurant site with (a) high (mean ΔOA
 257 $> 50 \mu g/m^3$) and (b) low (mean $\Delta OA < 30 \mu g/m^3$) enhancements grouped in each for
 258 comparison. The sample names in (a) and (b) are ordered by decreasing mean concentration.
 259

260 There is significant variability in measured ΔOA between and within each restaurant
 261 (Fig. 2 and Fig. S4). For nearly every location sampled, the emissions varied over time, as shown
 262 in Figure 1, and this contributes to wide interquartile ranges (IQRs) in Figure 2. It also means
 263 that at nearly every restaurant, there were periods when the concentration was near the urban
 264 background level, as indicated by the whiskers reaching (or even going slightly below) zero.

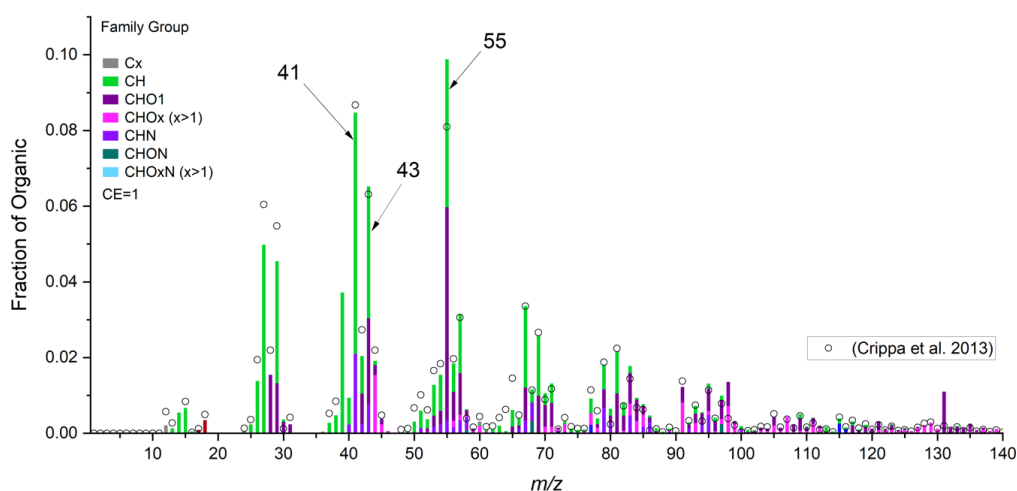
265 The temporal variability of the concentrations measured at each restaurant contributed to
 266 an upward skew in ΔOA , with a mean concentration greater than the 75th percentile at many
 267 locations. This suggests that the measurements were dominated by short, intense bursts of
 268 emissions rather than sustained high concentrations. Visualizations of this trend are noticeable in
 269 Figure 1b, where there is a large spike in emissions so that OA goes above $1000 \mu g/m^3$ for
 270 several minutes. The temporal variability seems to be associated with the quantity of cooking
 271 that spikes amid busy mealtimes.



272 Four restaurants were sampled on multiple days (Bar/Restaurant, Fast Food, Bakery, and
 273 Diner). While there were day-to-day differences in the mean ΔOA at each location, each of these
 274 locations fell into the same group (i.e., $\Delta OA < 30 \mu\text{g m}^{-3}$ or $\Delta OA > 50 \mu\text{g m}^{-3}$) on both sampling
 275 days. This suggests that the day-to-day variations in emissions are smaller than within-day
 276 emissions for each location and that high-emitting restaurants are consistently high emitters.
 277 However, due to the limitation of a single visit to each sampling location during the campaign, it
 278 may be challenging to conclusively ascertain that the classification assigned to the sampled
 279 restaurants is not indicative of all similar cooking operations.

280

281 3.3 OA composition across restaurants



282

283 **Figure 3.** Example mass spectrum from Bar/Restaurant 1 in this study and comparison with the
 284 COA mass spectrum from prior PMF work. High-resolution mass spectra are grouped into sticks
 285 of the unit mass resolution, and the coloring of each stick represents the mass fraction belonging to
 286 different chemical families.

287

288

289 In this section, we compare the composition of cooking OA across the restaurants and to

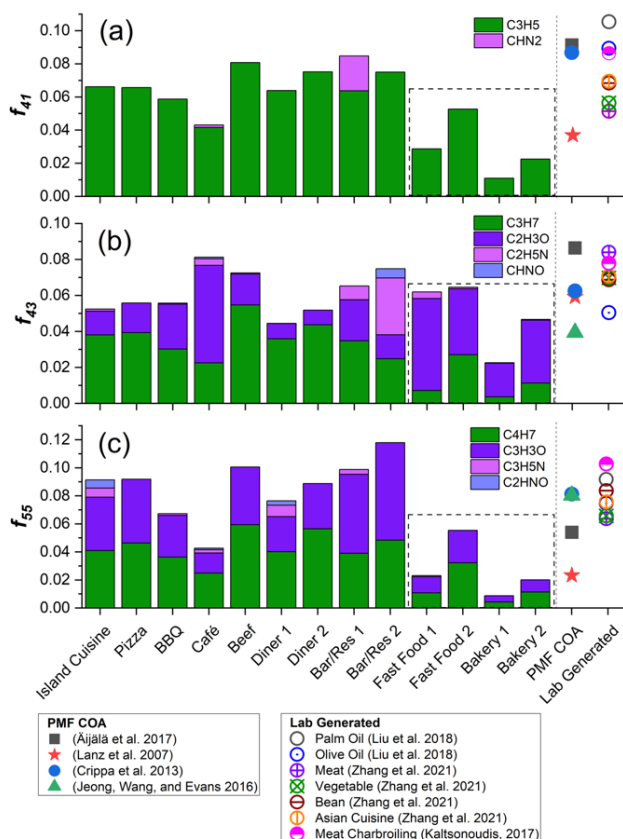
290 previous laboratory measurements and ambient factor analysis. Figure 3 shows the mean mass



291 spectrum of OA measured at Bar/Restaurant 1 in Baltimore; mass spectra from three additional
292 restaurants are shown in Figure S5. The mass spectrum contains a mixture of hydrocarbon
293 (C_xH_y) and oxygenated (C_xH_yO) ions. This is consistent with the composition of cooking OA,
294 which is often dominated by long-chain fatty acids from heated cooking oils and from meat
295 cooking (Crippa, DeCarlo, et al., 2013; D. D. Huang et al., 2021a; Liu et al., 2017; Mohr et al.,
296 2009; Takhar et al., 2019; Z. Zhang et al., 2021). Several lab experiments from seed oil cooking
297 detected fatty acids or degradation fragments such as *n*-alkanoic acid, *n*-alkenoic acid, oleic acid,
298 and carbonyls (Allan et al., 2010; Liu et al., 2018; Schauer et al., 2002). Unlike oils, which are
299 entirely comprised of fats, meats contain proteins and fats, although the composition can vary
300 depending on the type of meat. Cooking meat generally emits cholesterol and fatty acids like
301 palmitic acid, stearic acid, and oleic acid (Rogge et al., 1991a; Schauer et al., 1996), which have
302 all been used as chemical markers of meat cooking emissions. This mixture of hydrocarbon and
303 oxygenated ions is also identified in PMF factor analysis of ambient datasets, as indicated by the
304 mass spectrum from Crippa, DeCarlo, et al., (2013) shown in Figure 3.

305 The most abundant peaks in the mass spectrum were at m/z 41 (mostly $C_3H_5^+$), 43
306 ($C_2H_3O^+$ and $C_3H_7^+$), and 55 ($C_3H_3O^+$ and $C_4H_7^+$). These peaks have been used as COA markers
307 for tracing cooking sources in previous studies (Allan et al., 2010; Dall'Osto et al., 2015;
308 Kaltsonoudis et al., 2017; Mohr et al., 2009). Table 1 summarizes the mean contribution (f_{41} , f_{43} ,
309 and f_{55}) at these m/z to each restaurant's overall OA mass spectrum.

310



311

312 **Figure 4.** Fraction of (a) m/z 41, (b) 43, and (c) 55 to the total organic aerosol concentrations
 313 and comparison to COA mass spectra from prior PMF studies (Åijälä et al., 2017; Crippa,
 314 DeCarlo, et al., 2013; Jeong et al., 2016; Lanz et al., 2007) and laboratory-generated cooking
 315 emissions (Kaltsonoudis et al., 2017; Liu et al., 2018; Z. Zhang et al., 2021). Only f_{43} and f_{55}
 316 were shown in (Jeong et al., 2016) (f_{41} was not provided in the paper). Fast Food and Bakery
 317 samples are grouped in a box as they showed lower abundances of these common cooking
 318 marker fractions (f_{41} , f_{43} , and f_{55}).

319

320 Figure 4 compares f_{41} (OA mass fraction at m/z 41), f_{43} , and f_{55} across the restaurants
 321 sampled here to previously published COA mass spectra. We compared two types of previous
 322 studies: COA mass spectra derived from factor analysis of ambient data using PMF and
 323 laboratory measurements of cooking emissions. The laboratory measurements shown here



324 include a combination of heating palm and olive oils (Liu et al., 2018) and various cooking
325 experiments using meats (chicken and pork), vegetables, beans, and Asian cuisine (Kaltsonoudis
326 et al., 2017; Z. Zhang et al., 2021).

327 For m/z 41, our data were dominated by the hydrocarbon ion ($C_3H_5^+$), which was
328 approximately 4-8% of OA mass for most of the restaurants. The exceptions were Fast Food 1
329 and the two samples collected at the Bakery location. These had lower f_{41} (1-5%) and are shown
330 inside the dashed box. f_{41} fractions from our study were generally lower than from the PMF
331 COA factors. Three of the four COA factors have f_{41} of ~9% (Äijälä et al., 2017; Crippa,
332 DeCarlo, et al., 2013; Jeong et al., 2016). The COA factor from Lanz et al., 2007 is 4% and is
333 lower than most of the restaurants we sampled here. There is a wide range in f_{41} from the
334 laboratory experiments. The two oil heating experiments (palm and olive oil, Liu et al., 2018)
335 generated higher f_{41} than most of our measurements (8-10%). There was a wider range in f_{41} for
336 food cooking experiments (5-8%), and there is a strong overlap with our measurements.

337 For f_{43} and f_{55} , both oxidized (e.g., $C_2H_3O^+$ and $C_3H_3O^+$) and hydrocarbon (e.g., $C_3H_7^+$
338 and $C_4H_7^+$) ion fragments showed significant contributions across the urban cooking sites. There
339 were also minor contributions from nitrogen-containing ions (e.g., $C_2H_5N^+$ and C_2HNO^+). Except
340 for Bakery 1, f_{43} was ~5-8% in our measurements. However, there was variation in the relative
341 abundance of the hydrocarbon and oxygenated ions. For most sites, the contribution of the
342 hydrocarbon ($C_3H_7^+$) was larger than the oxygenated ion ($C_2H_3O^+$). However, the sites with low
343 f_{41} , Bakery and Fast Food 1, m/z 43 fragments were mostly oxygenated (mean = 3.5%).

344 The mean f_{43} in the PMF profiles was 6.3% with a range of 4-8.7%, which is similar to
345 the mean and range observed in our dataset. Similarly, the laboratory emissions data cluster

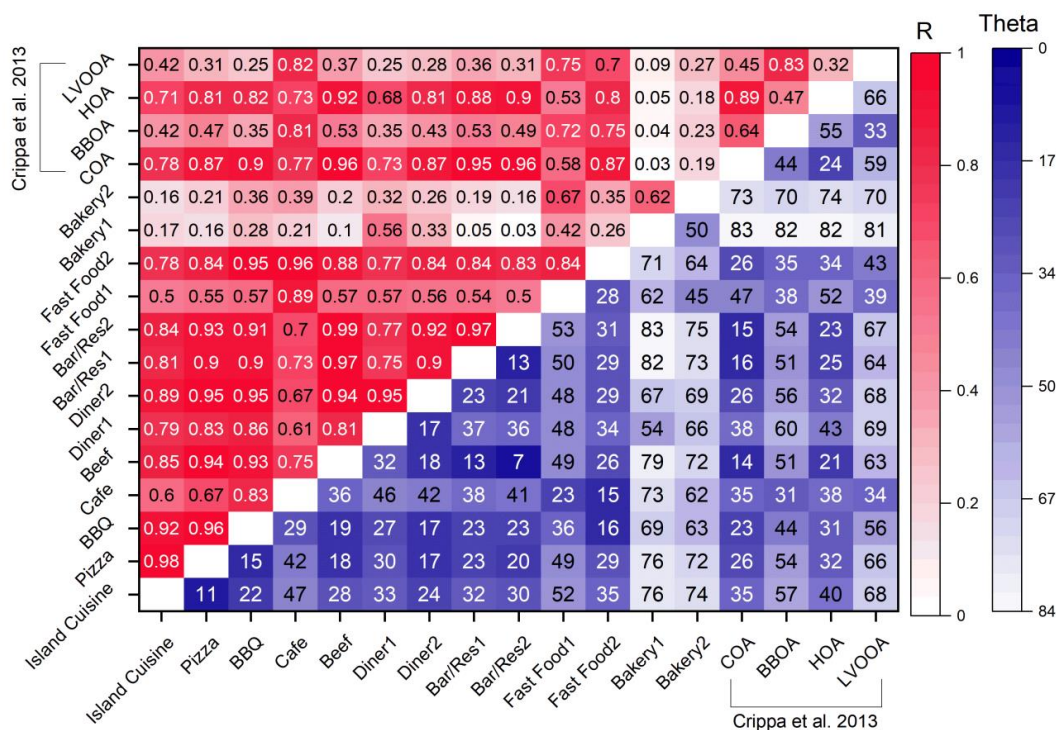


346 around f_{43} of 8%, with slightly lower f_{43} in the heated oil experiments. This is slightly higher
347 than the f_{43} measured in the restaurant emissions.

348 The pattern in f_{55} is similar to f_{43} ; contributions are dominated by the hydrocarbon and
349 oxygenated ion, with minor contributions from N-containing ions. For most sites, including the
350 Bakery and Fast Food sites, the contributions of hydrocarbon and oxygenated ions at m/z 55 are
351 similar. The largest difference is that the Bakery and Fast Food sites have significantly lower f_{55}
352 (1-6%) than the other sites (4-12%). Additionally, for many of the sites, f_{55} is larger than the
353 PMF factors and the laboratory experiments.

354 The variations in f_{41} , f_{43} , and f_{55} , as well as variations in the ratios between these m/z s,
355 may indicate the food cooked at the different restaurants. For example, f_{41} seems to be larger
356 than f_{43} for cooking emissions dominated by oil; this is the case in the oil heating experiments
357 from Liu et al. 2018 as well as from laboratory oil cooking emissions measured by Allan et al.
358 (Allan et al., 2010). Meat cooking emissions seem to have the opposite relationship, with $f_{43} >$
359 f_{41} . Both oil cooking and meat cooking have high f_{55} , and meat cooking may have $f_{55} > f_{43}$ (Mohr
360 et al., 2009).

361 For most restaurants sampled here (except Bakery and Fast Food), m/z 55 is the most
362 abundant signal in the aerosol mass spectrum. Additionally, f_{41} is slightly higher than f_{43} for
363 these sites. This suggests a mixture of meat and oil cooking at these locations. For Bakery and
364 Fast Food, f_{43} is typically the most abundant ion, with f_{41} exceeding f_{55} . This may suggest a
365 different mix of food being cooked, or a difference in the cooking style, however, there is
366 insufficient evidence in the mass spectra to conclusively explain the differences.



367

368 **Figure 5.** Comparison of the AMS UMR (unit mass resolution spectra) in two urban areas using
 369 correlation coefficients (R) and cosine similarity (θ , in degrees). R values close to 1 and θ values
 370 close to 0 mean strong correlations of mass spectra. Both R and θ values are presented such that
 371 darker colors correspond to higher similarity.
 372

373 Figure 4 compares the cooking OA mass spectra for specific marker ions. Figure 5
 374 compares the full cooking OA mass spectra. We use two metrics: the Pearson correlation (R) and
 375 cosine similarity. The statistical approach, correlation coefficient R, has been widely used in
 376 many studies, such as the analysis of air quality, to show an association between any two
 377 variables (Devarakonda et al., 2013; Giorio et al., 2012; Kiendler-Scharr et al., 2009;
 378 Raatikainen et al., 2010). Cosine similarity treats pairs of mass spectra as vectors and computes
 379 the angle (θ) between them (Kaltsonoudis et al., 2017; Kostenidou et al., 2009). θ is a measure of
 380 the similarities between two mass spectra, with a value of 0° , meaning that both spectra are



381 identical and $\theta > 30^\circ$ indicating considerable differences between the spectra. Cosine similarity is
382 more sensitive to smaller differences in mass spectra than R, as the correlation coefficient can be
383 dominated by ions with large abundance (Kaltsonoudis et al., 2017). Figure 5 also compares the
384 cooking emissions to PMF factors retrieved from Paris during winter (Crippa, DeCarlo, et al.,
385 2013) for biomass burning (BBOA), combustion emissions (HOA), and secondary OA
386 (LVOOA) obtained from the Jimenez Research Group website.
387 (<http://cires1.colorado.edu/jimenez-group/AMSsd/>).

388 Overall, the COA measured from most of the restaurants is similar. For most restaurants,
389 the R between mass spectra is larger than 0.8 and θ is less than 27° , suggesting that the mass
390 spectra are similar. Figures 3 and 4 show that the dominant ions in these mass spectra are at m/z
391 41, 43, and 55. The exceptions are the Bakery samples and, to a lesser extent, the Fast Food
392 samples. Bakery samples had $R < 0.3$ and $\theta > 50^\circ$ when compared to most of the other
393 restaurants. There were day-to-day differences in the Fast Food mass spectrum, with one day
394 (Fast Food 1) being similar to other restaurants ($R = 0.7-0.8$, $\theta < 30^\circ$), and the other day (Fast
395 Food 2) having lower R and higher θ . The following section discusses key mass spectral
396 differences in more detail.

397 There is also a high correlation of most restaurants with the COA PMF factor from
398 Crippa et al., (2013) ($R > \sim 0.75$, $\theta < \sim 30^\circ$). Correlations with BBOA and LVOOA are weaker as
399 these factors are characterized by dominant peaks at m/z 60 and 73 for BBOA and m/z 44 and 43
400 for LVOOA. There is a high R between our COA and the PMF HOA factor, which is
401 representative of primary combustion-related emissions. Even though m/z 41, 43, and 55 are
402 useful COA markers to resolve cooking-related factors, there are diverse sources of m/z 41, 43,
403 and 55. In general, there is a high correlation between HOA and COA because the major HOA



404 peaks like m/z 55 and 57 are prominent in both factors (Milic et al., 2016; Sun et al., 2013; D.
405 Yao et al., 2021).

406 One key difference between HOA and COA is that the HOA mass spectrum is dominated
407 by hydrocarbon (C_xH_y), whereas the cooking OA has a mixture of hydrocarbon and oxygenated
408 ions, as shown in Figure 4. For example, m/z 43 in HOA is almost entirely due to $C_3H_7^+$ (Ng et
409 al., 2010), whereas cooking OA contains both $C_3H_7^+$ and $C_2H_3O^+$ (Fig. 4). Similarly, for m/z 55,
410 COA has contributions from both hydrocarbon ($C_4H_7^+$) and oxidized ($C_3H_3O^+$) fragments
411 (Canonaco et al., 2013; Lalchandani et al., 2021), whereas the reduced ion dominates HOA.
412 Lastly, while m/z 55 and 57 are important signals for both COA and HOA, COA typically has f_{55}
413 $> f_{57}$, whereas HOA has the reverse (W. Hu et al., 2016; D. D. Huang et al., 2021a; Mohr et al.,
414 2009; Shah et al., 2018; Y. Zhang et al., 2015; Zhu et al., 2018).

415

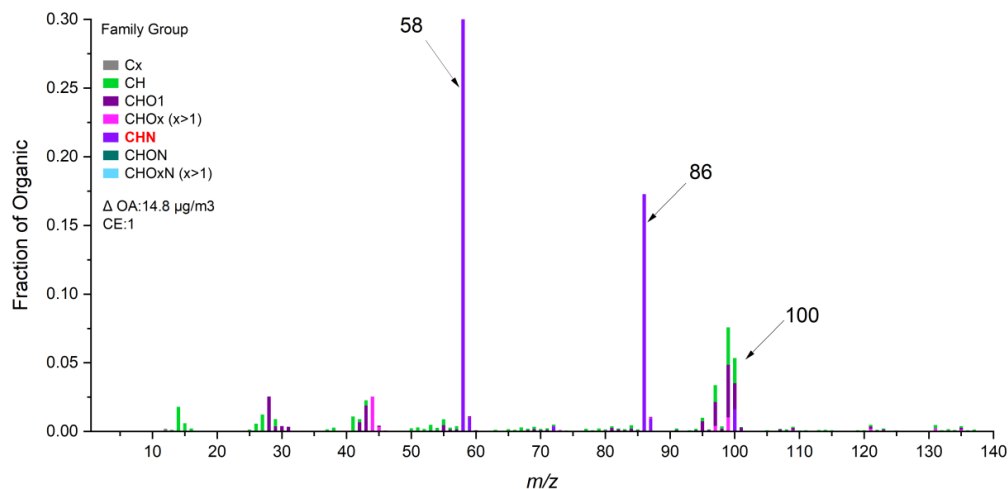
416 *3.4 Cooking as a source of urban reduced nitrogen*

417 Cooking OA from all of the restaurant sites had a significant contribution from AMS ions
418 containing reduced nitrogen. The mean contribution of nitrogen-containing fragments to the total
419 cooking OA mass was 15.8% (median = 10.7%; Table S2). The bulk of these N-containing ions
420 (95% by mass) did not contain oxygen (Fig. S6), though oxygen could still be present on the
421 parent molecule prior to fragmentation. These $C_xH_yN^+$ fragments include $C_2H_5N^+$ (m/z 43) and
422 $C_3H_5N^+$ (m/z 55), shown in Figure 4. For example, the mass spectrum from Bar/Restaurant 1 in
423 Figure 2 has 9% CHN family peaks by mass, with significant contributions at m/z 41 and 43. For
424 nearly all restaurants sampled here, the most abundant CHN group ion was $C_3H_8N^+$, with $f_{C_3H_8N}$
425 typically $> 1\%$.



426 Previous studies have reported the existence of nitrogen compounds or fragments from
427 cooking experiments. These nitrogen-containing compounds can originate from the food itself or
428 reactions with the types of gas used during cooking (Abdullahi et al., 2013). Reyes-Villegas et
429 al., 2018 measured gas- and particle-phase emissions and found 14 different nitrogen-containing
430 compounds using chemical ionization mass spectrometry. Rogge et al., 1991 measured amides in
431 cooking emissions, including palmitamide and steramide. Amides were also identified from both
432 Chinese cooking (Y. Zhao et al., 2007a) and Western-style cooking (Y. Zhao et al., 2007b) using
433 GC-MS. Ditto et al., (2022) recently demonstrated that amides can be formed from the reaction
434 of ammonia formed by amino acid thermal degradation with triglyceride ester linkages. In
435 contrast to the reduced nitrogen in our samples, these nitrogen-containing compounds, including
436 amides, have at least one oxygen in their formula.

437 The Bakery 1 and Bakery 2 samples had the largest contributions from reduced N. Figure
438 6 shows the aerosol mass spectrum from Bakery 1. The two most abundant ions in the mass
439 spectrum are $C_3H_8N^+$ (m/z 58) and $C_5H_{12}N^+$ (m/z 86); together these two ions make up ~48% of
440 the AMS-measured OA mass spectra. There is also a large contribution from $C_6H_{14}N^+$ at m/z 100.
441 The large abundance of these reduced N-containing peaks contributes to the low correlation
442 between the Bakery samples and other sites in Figure 5.



443
444 **Figure 6.** The aerosol mass spectrum from Barkery 1 with prominent peaks at m/z 58, 86, and
445 100 that are in the CHN family.
446

447 Though fast food sites have a lower correlation with other cooking sites in Figure 5, it is
448 not primarily due to higher CHN levels like bakery samples. The most abundant signals of Fast
449 Food 1 and Fast Food 2 were in the category of CHO and CH groups, where their sum accounts
450 for 73.3 % and 82.0 % of the total mass, respectively. Two samples from Fast Food sites show
451 moderate to slightly large proportions of CHN family peaks (14% and 7%) and $f_{C_3H_8N^+}$ (2.15 and
452 2.33).

453 While the $C_3H_8N^+$ fragment has been observed in all of our cooking site data, there is
454 almost no contribution of m/z 86 ($C_5H_{12}N^+$) and 100 ($C_6H_{14}N^+$) in our samples except for the two
455 bakery visits (Table S2), which were collected adjacent to a large commercial bread bakery. It is
456 thus possible that m/z 86 and 100 are more associated with commercial bakeries than restaurant
457 cooking. The underlying source of the reduced nitrogen ions, especially m/z 86 and 100 observed
458 at the bakery, is unknown. One potential source could be the use of azodicarbonamide
459 ($C_2H_4N_4O_2$, ADA), which is used as an aging and bleaching ingredient in bread baking. To test



460 whether ADA contributed to nitrogen-containing emissions from bread baking, we baked bread
461 with and without ADA addition. We used the AMS to measure the composition of PM emissions
462 during fermentation (i.e., while the bread dough rose) and baking. While we observed OA
463 emissions during baking, none of our experiments showed the CHN signals with $C_3H_8N^+$,
464 $C_5H_{12}N^+$, and $C_6H_{14}N^+$. As a result, we cannot conclude that the presence of ADA leads to high
465 proportions of CHN ions (SI Fig. 7).

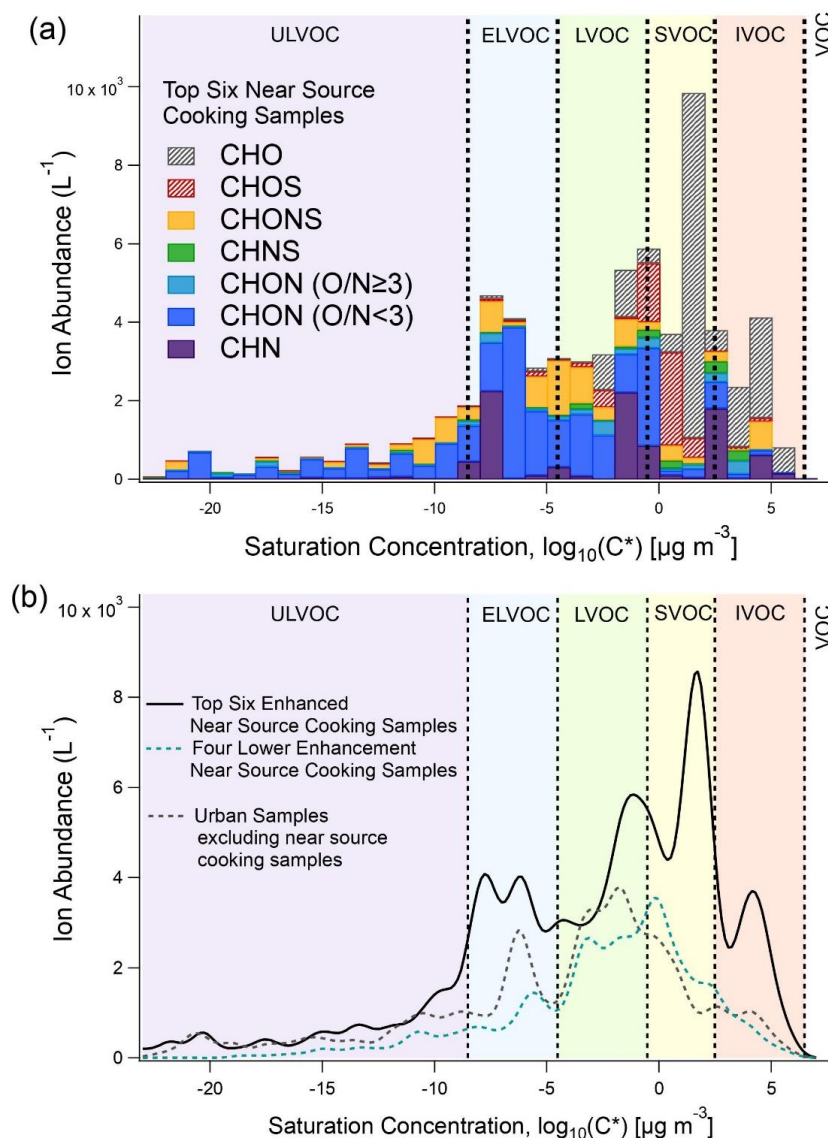
466 Abundant reduced nitrogen was also observed in the particle phase via LC-TOF and LC-
467 MS/MS measurements. To supplement the online measurements of functionalized aerosol-phase
468 compounds, especially those containing nitrogen, offline analysis using LC-TOF was employed
469 for organic compound speciation for each restaurant site with sufficient mass loading, with soft
470 ionization allowing for the molecular formula-level speciation of observed organic species.
471 Based on the online AMS data showing differences in OA enhancement (Fig. 2), the samples
472 were split into three sample groups, the six high-emitting restaurants (Bar/Res 1, Diner 2, Pizza,
473 Bar/Res 2, Diner 1, Island Cuisine), the lower enhancement near-source cooking samples
474 (Bakery 1, Bakery 2, Fast Food 1, Fast Food 2, Cafe), and urban samples excluding near-source
475 cooking samples (i.e., samples taken in different neighborhoods and parks), though this likely
476 includes cooking-related contributions to the urban background.

477 Figure 7a shows the ion abundance volatility distribution of the different functionalized
478 compound classes in the 6 samples with the highest PM concentrations (Fig. 2, see Fig. S10 for
479 other samples). Compound volatilities were estimated from the generated formulas, assuming all
480 species were at 300 K (Y. Li et al., 2016) from each sample, and all ion abundances were
481 normalized by the sample volume for comparison across samples. Figure 7b shows the volatility
482 distributions of ion abundances from the three sample groups, with the six more enhanced near-



483 source cooking samples demonstrating high ion abundance consistent with the higher mass
484 concentrations of PM_{2.5} sampled. The six enhanced cooking samples in Figure 7a show a greater
485 abundance of I/SVOCs compared to the other two sample groups, suggestive of fresh emissions.
486 The observed mixtures are highly functionalized, with observed species containing nitrogen,
487 oxygen, and sulfur, but we note that the LC-TOF employed here has poor ionization efficiencies
488 for CH and CHS compounds, which are thus not considered for this analysis of functionalized
489 compounds.

490 While urban particulate matter has been shown to contain many functionalized species
491 (Ditto et al., 2018; Ye et al., 2021), recent work has also shown cooking to be a source of
492 nitrogen and sulfur-containing species, which can be emitted in the gas-phase from foods such as
493 vegetables (Marcinkowska & Jeleń, 2022) or formed through cooking (Ditto et al., 2022; Takhar
494 et al., 2019). The urban background samples excluding cooking samples and the five lower
495 enhanced near-source cooking samples have similar volatility distributions with nitrogen-
496 containing compounds (Fig. 7b, S11), which suggests a role for cooking emissions in the
497 background functionalized OA composition in urban areas.



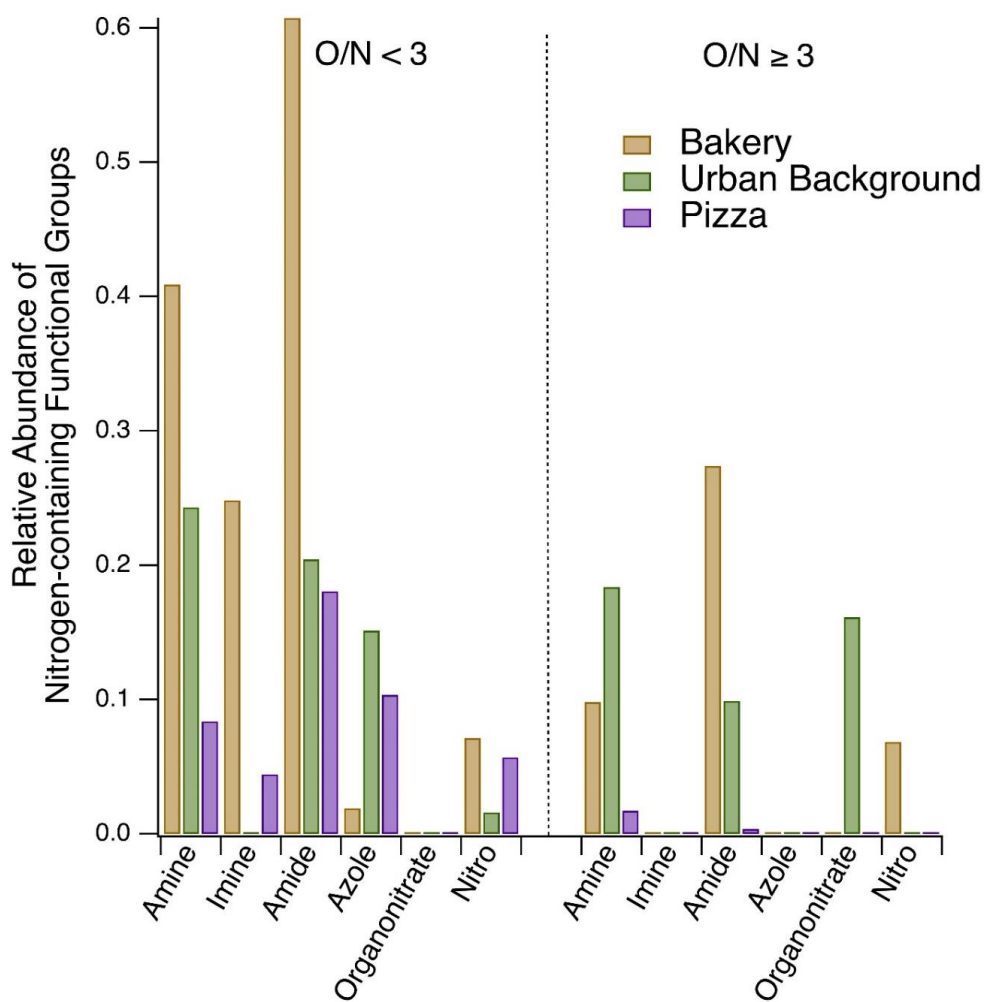
498

499 **Figure 7.** Averaged chemical composition of functionalized particle-phase organic compounds
 500 from (a) filters collected from the top six near-source cooking samples showing the highest
 501 enhancement in OA from the AMS measurements and (b) average ion abundance volatility
 502 distributions for the three sample groups, top six enhanced cooking samples, lower five near-
 503 source cooking samples, and the urban samples excluding near source cooking samples.
 504 Volatility bins were defined for the same reference temperature in (a) and (b) (i.e., 300 K, as all
 505 samples were collected during summertime).
 506



507 While all samples contained nitrogen-containing compounds, LC-MS/MS was used on
508 select samples (Bakery 1, Pizza, background sample 5) from each sample group to compare the
509 functionalities of observed nitrogen. After compounds observed via LC-TOF (i.e., Fig. 7a)
510 underwent QC/QA, those compounds were selected for MS/MS analysis in a targeted mode
511 similar to prior work (Ditto et al., 2020).

512 Most nitrogen-containing compounds observed had an O/N of less than 3, but other
513 nitrogen-containing compound classes were present (Fig. 7, S11). Figure 8 shows the observed
514 nitrogen-containing functional groups for the three samples run on MS/MS, split by O/N ratio
515 less than 3 or greater than or equal to 3. Here, the Bakery 1 compounds analyzed by MS/MS
516 were dominated by reduced nitrogen features, with prominent amine and amide functional
517 groups, especially for compounds with O/N ratios lower than 3, which in itself is indicative of
518 the presence of reduced nitrogen structural features.



519

520 **Figure 8.** The relative abundance of nitrogen-containing functionalities in the Bakery 1,
 521 background sample 5, and Pizza MS/MS compounds are shown, separated by O/N ratio <3 on
 522 the left and ≥ 3 on the right, with prominently reduced nitrogen functionalities in the bakery
 523 sample. See Figure S13 for the complete range of functional groups and structural features
 524 observed in these samples. Enamine, nitrophenol, and nitrile functionalities were also searched
 525 for but were not detected in these three samples.

526

527

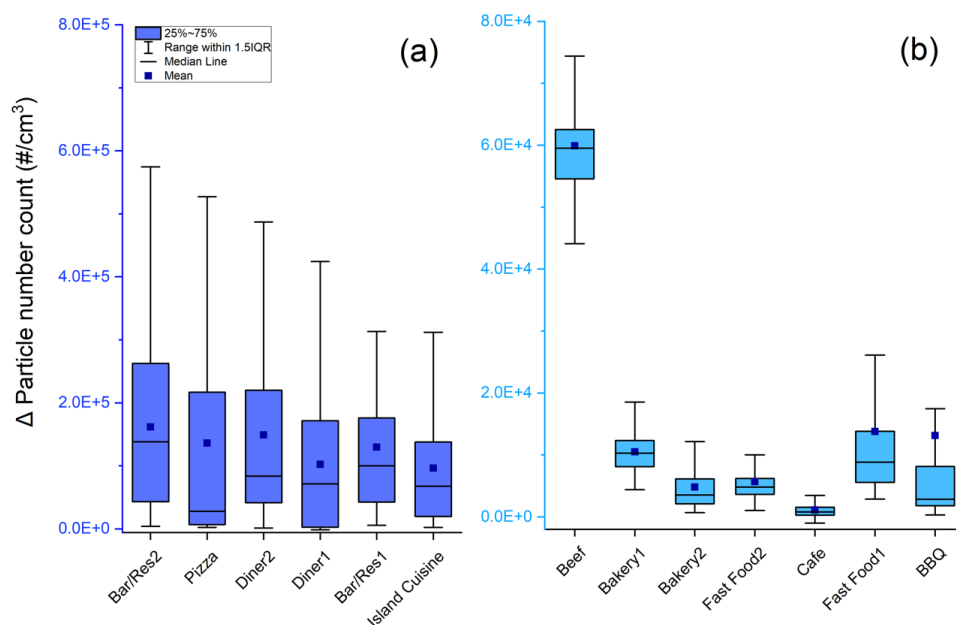
528

529



530 3.5. Particle size distributions and UFP enhancements in restaurant plumes

531 To expand upon Figure 1’s observations of UFPs in an example restaurant plume, we
 532 examined UFP enhancements across the sampled restaurants and the size distribution of those
 533 emissions.



534

535 **Figure 9.** Particle number enhancement (Δ PNC) at each restaurant site (with IQR). The sample
 536 names in (a) and (b) are placed in the same order as in Figure 2.

537

538

539

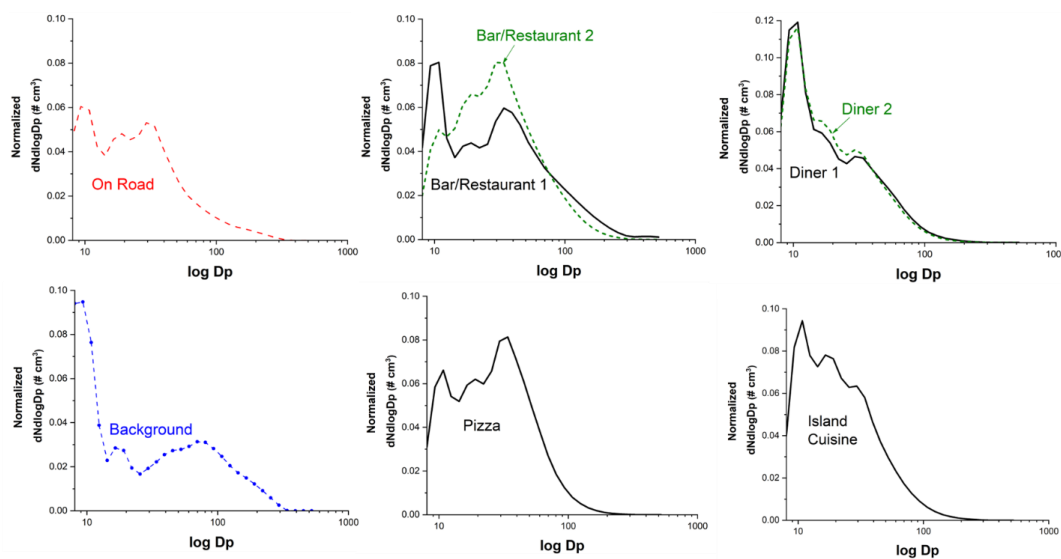
Figure 9 summarizes the particle number concentrations above the background (Δ PNC)
 540 measured by the FMPS and scaled to the CPC. Similar to our Δ OA distribution in Figure 2, there
 541 are notable site-to-site differences in particle number concentrations with the sites breaking down
 542 into the higher and lower-emitting groups (high Δ PNC group mean Δ PNC $> 10^5 \#/cm^3$, low
 543 Δ PNC group mean Δ PNC $< 10^5 \#/cm^3$).



544 All of the high Δ PNC sites were also high Δ OA sites, but most sites do not have a strong
545 correlation between mean Δ OA and mean Δ PNC (Fig. S8). A moderate positive correlation was
546 observed in the time series of PNC and OA at Diner 1 ($R^2 = 0.64$), Beef (0.63), Bar/Restaurant 2
547 (0.60), and Bakery 1 (0.57); most other sites had poor correlations between Δ OA and Δ PNC (R^2
548 < 0.4). This poor correlation may indicate that the emissions of OA and PNC are decoupled
549 during cooking so that different activities boost emissions of OA mass versus particle number.
550 For example, the PNC time series in Figure 1 has several spikes that do not have associated
551 spikes in OA.

552 The PNC enhancements are less skewed than the OA enhancements. For Δ PNC, the
553 mean is always inside the IQR except for the BBQ sample, unlike several sites that had mean
554 Δ OA $> 75^{\text{th}}$ percentile. This implies that PNC emissions are less dominated by intense spikes
555 than OA emissions. Figure 2 and Figure S4 show that OA concentrations often fell close to the
556 background between spikes. PNC, on the other hand, was consistently elevated during the
557 restaurant sampling. One possible explanation is that OA spikes are associated with cooking,
558 whereas the consistently high PNC is associated with the heating of the cooking surface by either
559 a natural gas flame or electricity (Amouei Torkmahalleh et al., 2018; Dennekamp et al., 2001;
560 Wu et al., 2012).

561



562

563 **Figure 10.** Mean particle size distribution comparison of on-road, background, and high Δ PNC
 564 restaurants observed at Bar/Restaurant, Diner, Pizza, and Island cuisine measured from the
 565 FMPS (Fast Mobility Particle Sizer). To fit the size distributions onto the same scale, all are
 566 normalized to the total particle number ($dN/d\log D_p$) of each sampling period over each size bin
 567 and make the sum of all normalized size distributions to be 1.
 568

569 Figure 10 shows the mean particle size distributions for the “high Δ PNC” restaurants
 570 from Figure 7a and the mean on-road and background particle size distributions from the period
 571 shown in Figure 1. All the restaurants emitted UFPs. The mode particle diameter from all
 572 sampled restaurants was less than 50 nm (Table 1), and the size distributions in Figure 10 clearly
 573 peak in the ultrafine size range. However, there is variability across the restaurants as some sites
 574 had bimodal size distributions, while others are closer to unimodal. For example, Bar/Restaurant
 575 1 has distinct modes at ~10 and 40 nm, whereas Island Cuisine has a single broad mode centered
 576 around 20 nm. There is also variability within sites. For example, Bar/Restaurant 2 has a
 577 unimodal distribution with a mode around 40 nm, and the size distribution differs from the other



578 sample at the same location, while the two samples at the Diner have nearly identical size
579 distributions.

580 In addition to being enhanced in terms of concentrations, the size distributions in the
581 restaurant plumes are distinct from the average background size distributions, which have a
582 bimodal distribution with a nucleation mode peak around 10 nm and an accumulation mode peak
583 around 100 nm. Emissions from nearby vehicles dominate the on-road periods, with a bimodal
584 size distribution around 10 nm and 20-40 nm, which is similarly observed in previous studies
585 (Sturm et al., 2003; Wang et al., 2008; X. Yao et al., 2005).

586

587 **4. Conclusions and Atmospheric Relevance**

588 Using mobile measurements across a range of commercial cooking operations in two
589 cities, our real-world sampling of cooking plumes from restaurants demonstrates substantial
590 cooking-associated aerosol emissions with variability in the concentrations, chemical
591 composition, and size distribution of PM and UFP emissions. Reduced nitrogen (N) was
592 prevalent across all restaurant samples, contributing approximately 15% of the cooking organic
593 aerosol (OA) mass at the sampled sites, with a diversity of reduced N functional groups
594 observed. However, a notable finding of this study was the distinct composition of emissions
595 collected from a commercial bakery, marked by the elevated presence of reduced nitrogen.
596 Numerous studies have investigated cooking aerosol compositions, demonstrating that different
597 cooking techniques and ingredients can elevate nitrogen content levels (Ditto et al., 2022;
598 Masoud et al., 2022; Reyes-Villegas et al., 2018b; Rogge et al., 1991b). Nitrogen found in
599 cooking emissions has diverse origins, including from the food itself with both natural (e.g.,
600 protein-rich and plant-based products) (Bak et al., 2019; Han et al., 2020) and anthropogenic



601 sources (e.g., fertilizers and food additives like nitrates and nitrites) (Dimkpa et al., 2020;
602 Karwowska & Kononiuk, 2020), as well as from nitrogen dioxide (NO₂) and other nitrogen
603 oxides (NO_x) emitted from gas cooking burners (H. Zhao et al., 2021), which are primarily
604 influenced by the duration of gas cooking and the ambient air quality (Mosqueron et al., 2002).
605 To further examine potential sources of the nitrogen features identified from the bakery
606 emissions, we conducted an experiment with the AMS measuring bread baking emissions both
607 with and without the dough stabilizer azodicarbonamide (C₂H₄N₄O₂) as a potential source of N-
608 containing peaks. While the reduced nitrogen peaks were not observed, this result implies the
609 challenge in determining specific sources of nitrogen-containing species, particularly in real-
610 world cooking environments, emphasizing the need for further investigation.

611 This study also highlights that cooking emissions are substantial contributors to urban
612 UFPs. Variability between sites was observed, with some sites displaying unimodal and others
613 displaying bimodal size distributions. However, there are uncertainties in identifying the
614 characteristics of UFPs from cooking emissions, such as their origin from cooking processes or
615 natural gas usage, and potential changes in particle size distributions during dilution due to the
616 evaporation of semi-volatile components. Uncontrolled dilution in this study may have
617 contributed to differences in UFP concentration and size distribution (Lipsky & Robinson, 2006).

618 While it is acknowledged that a proportion of cooking emissions may undergo
619 evaporation during the dilution process, it is improbable that these particles will evaporate
620 entirely. Previous research conducted by Louvaris et al (Louvaris et al., 2017) investigated meat
621 charbroiling emissions diluted within a chamber and reported that approximately 80% of the
622 COA persisted following isothermal dilution at ambient temperature (25 °C) by a factor of 10. In
623 order to gain a deeper understanding of the factors influencing UFP size distribution from real-



624 world cooking sources, further investigation is warranted, taking into account aspects such as
625 restaurant proximity, food type, and order frequency. Consequently, subsequent research can
626 identify the prevalent molecular features of reduced nitrogen in cooking emissions by setting
627 constraints on specific parameters, providing a more comprehensive analysis.

628 Overall, this study underscores the importance of comprehensively understanding
629 cooking emissions, including their contribution to the $PM_{2.5}$ mass, composition, and exposure
630 variability across urban areas, in order to develop effective strategies for mitigating their impact
631 on air quality and human health. Specifically, further research is needed to better understand the
632 role of reduced nitrogen in atmospheric emissions from cooking activities.

633

634

635 *Data availability.* All data presented in this work can be obtained by directly contacting the
636 corresponding author at apresto@andrew.cmu.edu upon request.

637

638 *Author contributions.* The experimental design was done by AAP and DRG. Data collection was
639 carried out by AAP and JEM. SK performed the data analysis and compiled the instrumental
640 data. SK and AAP wrote the paper, with all authors contributing significantly to the
641 interpretation of the results, discussions, and finalization of the paper.

642

643 *Competing interests.* At least one of the (co-)authors is a member of the editorial board of
644 Atmospheric Chemistry and Physics. The peer-review process was guided by an independent
645 editor, and the authors also have no other competing interests to declare.

646



647
648 *Acknowledgments.* This research was conducted as part of the Center for Air, Climate, and
649 Energy Solutions (CACES), which was supported by the Environmental Protection Agency
650 (assistance agreement number RD83587301) to Carnegie Mellon University. We
651 acknowledge support from assistance agreement no. RD835871 awarded by the U.S.
652 Environmental Protection Agency to Yale University. This study has not been formally reviewed
653 by the EPA. The views expressed in this document are solely those of the authors and do not
654 necessarily reflect those of the agency. The EPA does not endorse any products or commercial
655 services mentioned in this publication. DRG and JEM acknowledge financial support from the
656 U.S. NSF (CBET-2011362). SK and AAP acknowledge funding support from the U.S. NSF
657 (CBET 1907446)

658

659

660 *References*

661

662 Abdullahi, K. L., Delgado-Saborit, J. M., & Harrison, R. M. (2013). Emissions and indoor
663 concentrations of particulate matter and its specific chemical components from cooking:
664 A review. *Atmospheric Environment*, 71, 260–294.
665 <https://doi.org/10.1016/j.atmosenv.2013.01.061>

666 Äijälä, M., Heikkinen, L., Fröhlich, R., Canonaco, F., Prévôt, A. S. H., Junninen, H., Petäjä, T.,
667 Kulmala, M., Worsnop, D., & Ehn, M. (2017). Resolving anthropogenic aerosol pollution
668 types – deconvolution and exploratory classification of pollution events. *Atmospheric
669 Chemistry and Physics*, 17(4), 3165–3197. <https://doi.org/10.5194/acp-17-3165-2017>



- 670 Ali, M. U., Lin, S., Yousaf, B., Abbas, Q., Munir, M. A. M., Rashid, A., Zheng, C., Kuang, X.,
671 & Wong, M. H. (2022). Pollution characteristics, mechanism of toxicity and health
672 effects of the ultrafine particles in the indoor environment: Current status and future
673 perspectives. *Critical Reviews in Environmental Science and Technology*, 52(3), 436–
674 473. <https://doi.org/10.1080/10643389.2020.1831359>
- 675 Allan, J. D., Williams, P. I., Morgan, W. T., Martin, C. L., Flynn, M. J., Lee, J., Nemitz, E.,
676 Phillips, G. J., Gallagher, M. W., & Coe, H. (2010). Contributions from transport, solid
677 fuel burning and cooking to primary organic aerosols in two UK cities. *Atmospheric
678 Chemistry and Physics*, 10(2), 647–668. <https://doi.org/10.5194/acp-10-647-2010>
- 679 Amouei Torkmahalleh, M., Ospanova, S., Baibatyrova, A., Nurbay, S., Zhanakhmet, G., & Shah,
680 D. (2018). Contributions of burner, pan, meat and salt to PM emission during grilling.
681 *Environmental Research*, 164, 11–17. <https://doi.org/10.1016/j.envres.2018.01.044>
- 682 Apte, J. S., Messier, K. P., Gani, S., Brauer, M., Kirchstetter, T. W., Lunden, M. M., Marshall, J.
683 D., Portier, C. J., Vermeulen, R. C. H., & Hamburg, S. P. (2017). High-Resolution Air
684 Pollution Mapping with Google Street View Cars: Exploiting Big Data. *Environmental
685 Science & Technology*, 51(12), 6999–7008. <https://doi.org/10.1021/acs.est.7b00891>
- 686 Bak, U. G., Nielsen, C. W., Marinho, G. S., Gregersen, Ó., Jónsdóttir, R., & Holdt, S. L. (2019).
687 The seasonal variation in nitrogen, amino acid, protein and nitrogen-to-protein
688 conversion factors of commercially cultivated Faroese *Saccharina latissima*. *Algal
689 Research*, 42, 101576. <https://doi.org/10.1016/j.algal.2019.101576>
- 690 Bozzetti, C., El Haddad, I., Salameh, D., Daellenbach, K. R., Fermo, P., Gonzalez, R.,
691 Minguillón, M. C., Iinuma, Y., Poulain, L., Elser, M., Müller, E., Slowik, J. G., Jaffrezo,
692 J.-L., Baltensperger, U., Marchand, N., & Prévôt, A. S. H. (2017). Organic aerosol source



693 apportionment by offline-AMS over a full year in Marseille. *Atmospheric Chemistry and*
694 *Physics*, 17(13), 8247–8268. <https://doi.org/10.5194/acp-17-8247-2017>

695 Canonaco, F., Crippa, M., Slowik, J. G., Baltensperger, U., & Prévôt, A. S. H. (2013). SoFi, an
696 IGOR-based interface for the efficient use of the generalized multilinear engine (ME-2)
697 for the source apportionment: ME-2 application to aerosol mass spectrometer data.
698 *Atmospheric Measurement Techniques*, 6(12), 3649–3661. [https://doi.org/10.5194/amt-6-](https://doi.org/10.5194/amt-6-3649-2013)
699 3649-2013

700 Castillo, M. D., Kinney, P. L., Southerland, V., Arno, C. A., Crawford, K., van Donkelaar, A.,
701 Hammer, M., Martin, R. V., & Anenberg, S. C. (2021). Estimating Intra-Urban Inequities
702 in PM_{2.5}-Attributable Health Impacts: A Case Study for Washington, DC. *GeoHealth*,
703 5(11), e2021GH000431. <https://doi.org/10.1029/2021GH000431>

704 Cheng, B., Wang-Li, L., Meskhidze, N., Classen, J., & Bloomfield, P. (2019). Spatial and
705 temporal variations of PM_{2.5} mass closure and inorganic PM_{2.5} in the Southeastern U.S.
706 *Environmental Science and Pollution Research*, 26(32), 33181–33191.
707 <https://doi.org/10.1007/s11356-019-06437-8>

708 Chow, J. C., Chen, L.-W. A., Watson, J. G., Lowenthal, D. H., Magliano, K. A., Turkiewicz, K.,
709 & Lehrman, D. E. (2006). PM_{2.5} chemical composition and spatiotemporal variability
710 during the California Regional PM₁₀/PM_{2.5} Air Quality Study (CRPAQS). *Journal of*
711 *Geophysical Research: Atmospheres*, 111(D10). <https://doi.org/10.1029/2005JD006457>

712 Crippa, M., DeCarlo, P. F., Slowik, J. G., Mohr, C., Heringa, M. F., Chirico, R., Poulain, L.,
713 Freutel, F., Sciare, J., Cozic, J., Di Marco, C. F., Elsasser, M., Nicolas, J. B., Marchand,
714 N., Abidi, E., Wiedensohler, A., Drewnick, F., Schneider, J., Borrmann, S., ...
715 Baltensperger, U. (2013). Wintertime aerosol chemical composition and source



- 716 apportionment of the organic fraction in the metropolitan area of Paris. *Atmospheric*
717 *Chemistry and Physics*, 13(2), 961–981. <https://doi.org/10.5194/acp-13-961-2013>
- 718 Crippa, M., El Haddad, I., Slowik, J. G., DeCarlo, P. F., Mohr, C., Heringa, M. F., Chirico, R.,
719 Marchand, N., Sciare, J., Baltensperger, U., & Prévôt, A. S. H. (2013). Identification of
720 marine and continental aerosol sources in Paris using high resolution aerosol mass
721 spectrometry. *Journal of Geophysical Research: Atmospheres*, 118(4), 1950–1963.
722 <https://doi.org/10.1002/jgrd.50151>
- 723 Dallmann, T. R., Kirchstetter, T. W., DeMartini, S. J., & Harley, R. A. (2013). Quantifying On-
724 Road Emissions from Gasoline-Powered Motor Vehicles: Accounting for the Presence of
725 Medium- and Heavy-Duty Diesel Trucks. *Environmental Science & Technology*, 47(23),
726 13873–13881. <https://doi.org/10.1021/es402875u>
- 727 Dall’Osto, M., Paglione, M., Decesari, S., Facchini, M. C., O’Dowd, C., Plass-Duellmer, C., &
728 Harrison, R. M. (2015). On the Origin of AMS “Cooking Organic Aerosol” at a Rural
729 Site. *Environmental Science & Technology*, 49(24), 13964–13972.
730 <https://doi.org/10.1021/acs.est.5b02922>
- 731 Dennekamp, M., Howarth, S., Dick, C. a. J., Cherrie, J. W., Donaldson, K., & Seaton, A. (2001).
732 Ultrafine particles and nitrogen oxides generated by gas and electric cooking.
733 *Occupational and Environmental Medicine*, 58(8), 511–516.
734 <https://doi.org/10.1136/oem.58.8.511>
- 735 Devarakonda, S., Sevusu, P., Liu, H., Liu, R., Iftode, L., & Nath, B. (2013). Real-time air quality
736 monitoring through mobile sensing in metropolitan areas. *Proceedings of the 2nd ACM*
737 *SIGKDD International Workshop on Urban Computing*, 1–8.
738 <https://doi.org/10.1145/2505821.2505834>



- 739 Dimkpa, C. O., Fugice, J., Singh, U., & Lewis, T. D. (2020). Development of fertilizers for
740 enhanced nitrogen use efficiency – Trends and perspectives. *Science of The Total*
741 *Environment*, 731, 139113. <https://doi.org/10.1016/j.scitotenv.2020.139113>
- 742 Ditto, J. C., Abbatt, J. P. D., & Chan, A. W. H. (2022). Gas- and Particle-Phase Amide
743 Emissions from Cooking: Mechanisms and Air Quality Impacts. *Environmental Science*
744 *& Technology*, 56(12), 7741–7750. <https://doi.org/10.1021/acs.est.2c01409>
- 745 Ditto, J. C., Barnes, E. B., Khare, P., Takeuchi, M., Joo, T., Bui, A. A. T., Lee-Taylor, J., Eris,
746 G., Chen, Y., Aumont, B., Jimenez, J. L., Ng, N. L., Griffin, R. J., & Gentner, D. R.
747 (2018). An omnipresent diversity and variability in the chemical composition of
748 atmospheric functionalized organic aerosol. *Communications Chemistry*, 1(1), Article 1.
749 <https://doi.org/10.1038/s42004-018-0074-3>
- 750 Ditto, J. C., Joo, T., Slade, J. H., Shepson, P. B., Ng, N. L., & Gentner, D. R. (2020).
751 Nontargeted Tandem Mass Spectrometry Analysis Reveals Diversity and Variability in
752 Aerosol Functional Groups across Multiple Sites, Seasons, and Times of Day.
753 *Environmental Science & Technology Letters*, 7(2), 60–69.
754 <https://doi.org/10.1021/acs.estlett.9b00702>
- 755 Dührkop, K., Fleischauer, M., Ludwig, M., Aksenov, A. A., Melnik, A. V., Meusel, M.,
756 Dorrestein, P. C., Rousu, J., & Böcker, S. (2019). SIRIUS 4: A rapid tool for turning
757 tandem mass spectra into metabolite structure information. *Nature Methods*, 16(4),
758 Article 4. <https://doi.org/10.1038/s41592-019-0344-8>
- 759 Dührkop, K., Shen, H., Meusel, M., Rousu, J., & Böcker, S. (2015). Searching molecular
760 structure databases with tandem mass spectra using CSI:FingerID. *Proceedings of the*



- 761 *National Academy of Sciences*, 112(41), 12580–12585.
762 <https://doi.org/10.1073/pnas.1509788112>
- 763 Florou, K., Papanastasiou, D. K., Pikridas, M., Kaltsonoudis, C., Louvaris, E., Gkatzelis, G. I.,
764 Patoulis, D., Mihalopoulos, N., & Pandis, S. N. (2017). The contribution of wood
765 burning and other pollution sources to wintertime organic aerosol levels in two Greek
766 cities. *Atmospheric Chemistry and Physics*, 17(4), 3145–3163.
767 <https://doi.org/10.5194/acp-17-3145-2017>
- 768 Font, A., Guiseppin, L., Blangiardo, M., Ghersi, V., & Fuller, G. W. (2019). A tale of two cities:
769 Is air pollution improving in Paris and London? *Environmental Pollution*, 249, 1–12.
770 <https://doi.org/10.1016/j.envpol.2019.01.040>
- 771 Giorio, C., Tapparo, A., Dall’Osto, M., Harrison, R. M., Beddows, D. C. S., Di Marco, C., &
772 Nemitz, E. (2012). Comparison of three techniques for analysis of data from an Aerosol
773 Time-of-Flight Mass Spectrometer. *Atmospheric Environment*, 61, 316–326.
774 <https://doi.org/10.1016/j.atmosenv.2012.07.054>
- 775 Han, Y., Feng, G., Swaney, D. P., Dentener, F., Koeble, R., Ouyang, Y., & Gao, W. (2020).
776 Global and regional estimation of net anthropogenic nitrogen inputs (NANI). *Geoderma*,
777 361, 114066. <https://doi.org/10.1016/j.geoderma.2019.114066>
- 778 Hayes, P. L., Ortega, A. M., Cubison, M. J., Froyd, K. D., Zhao, Y., Cliff, S. S., Hu, W. W.,
779 Toohey, D. W., Flynn, J. H., Lefer, B. L., Grossberg, N., Alvarez, S., Rappenglück, B.,
780 Taylor, J. W., Allan, J. D., Holloway, J. S., Gilman, J. B., Kuster, W. C., de Gouw, J. A.,
781 ... Jimenez, J. L. (2013). Organic aerosol composition and sources in Pasadena,
782 California, during the 2010 CalNex campaign. *Journal of Geophysical Research:*
783 *Atmospheres*, 118(16), 9233–9257. <https://doi.org/10.1002/jgrd.50530>



- 784 Hering, S. V., Lewis, G. S., Spielman, S. R., & Eiguren-Fernandez, A. (2019). A MAGIC
785 concept for self-sustained, water-based, ultrafine particle counting. *Aerosol Science and*
786 *Technology*, 53(1), 63–72. <https://doi.org/10.1080/02786826.2018.1538549>
- 787 Hu, R., Wang, S., Zheng, H., Zhao, B., Liang, C., Chang, X., Jiang, Y., Yin, R., Jiang, J., & Hao,
788 J. (2021). Variations and Sources of Organic Aerosol in Winter Beijing under Markedly
789 Reduced Anthropogenic Activities During COVID-2019. *Environmental Science &*
790 *Technology*. <https://doi.org/10.1021/acs.est.1c05125>
- 791 Hu, W., Hu, M., Hu, W., Jimenez, J. L., Yuan, B., Chen, W., Wang, M., Wu, Y., Chen, C.,
792 Wang, Z., Peng, J., Zeng, L., & Shao, M. (2016). Chemical composition, sources, and
793 aging process of submicron aerosols in Beijing: Contrast between summer and winter.
794 *Journal of Geophysical Research: Atmospheres*, 121(4), 1955–1977.
795 <https://doi.org/10.1002/2015JD024020>
- 796 Huang, D. D., Zhu, S., An, J., Wang, Q., Qiao, L., Zhou, M., He, X., Ma, Y., Sun, Y., Huang, C.,
797 Yu, J. Z., & Zhang, Q. (2021b). Comparative Assessment of Cooking Emission
798 Contributions to Urban Organic Aerosol Using Online Molecular Tracers and Aerosol
799 Mass Spectrometry Measurements. *Environmental Science & Technology*, 55(21),
800 14526–14535. <https://doi.org/10.1021/acs.est.1c03280>
- 801 Huang, X.-F., He, L.-Y., Hu, M., Canagaratna, M. R., Sun, Y., Zhang, Q., Zhu, T., Xue, L.,
802 Zeng, L.-W., Liu, X.-G., Zhang, Y.-H., Jayne, J. T., Ng, N. L., & Worsnop, D. R. (2010).
803 Highly time-resolved chemical characterization of atmospheric submicron particles
804 during 2008 Beijing Olympic Games using an Aerodyne High-Resolution Aerosol Mass
805 Spectrometer. *Atmospheric Chemistry and Physics*, 10(18), 8933–8945.
806 <https://doi.org/10.5194/acp-10-8933-2010>



- 807 Ibalid-Mulli, A., Wichmann, H.-E., Kreyling, W., & Peters, A. (2002). Epidemiological Evidence
808 on Health Effects of Ultrafine Particles. *Journal of Aerosol Medicine*, 15(2), 189–201.
809 <https://doi.org/10.1089/089426802320282310>
- 810 Jeong, C.-H., Wang, J. M., & Evans, G. J. (2016). Source Apportionment of Urban Particulate
811 Matter using Hourly Resolved Trace Metals, Organics, and Inorganic Aerosol
812 Components. *Atmospheric Chemistry and Physics Discussions*, 1–32.
813 <https://doi.org/10.5194/acp-2016-189>
- 814 Jung, C.-C., & Su, H.-J. (2020). Chemical and stable isotopic characteristics of PM_{2.5} emitted
815 from Chinese cooking. *Environmental Pollution*, 267, 115577.
816 <https://doi.org/10.1016/j.envpol.2020.115577>
- 817 Kaltsonoudis, C., Kostenidou, E., Louvaris, E., Psychoudaki, M., Tsiligiannis, E., Florou, K.,
818 Liangou, A., & Pandis, S. N. (2017). Characterization of fresh and aged organic aerosol
819 emissions from meat charbroiling. *Atmospheric Chemistry and Physics*, 17(11), 7143–
820 7155. <https://doi.org/10.5194/acp-17-7143-2017>
- 821 Karwowska, M., & Kononiuk, A. (2020). Nitrates/Nitrites in Food—Risk for Nitrosative Stress
822 and Benefits. *Antioxidants*, 9(3), Article 3. <https://doi.org/10.3390/antiox9030241>
- 823 Keuken, M. P., Roemer, M. G. M., Zandveld, P., Verbeek, R. P., & Velders, G. J. M. (2012).
824 Trends in primary NO₂ and exhaust PM emissions from road traffic for the period 2000–
825 2020 and implications for air quality and health in the Netherlands. *Atmospheric
826 Environment*, 54, 313–319. <https://doi.org/10.1016/j.atmosenv.2012.02.009>
- 827 Kiendler-Scharr, A., Zhang, Q., Hohaus, T., Kleist, E., Mensah, A., Mentel, T. F., Spindler, C.,
828 Uerlings, R., Tillmann, R., & Wildt, J. (2009). Aerosol Mass Spectrometric Features of
829 Biogenic SOA: Observations from a Plant Chamber and in Rural Atmospheric



- 830 Environments. *Environmental Science & Technology*, 43(21), 8166–8172.
831 <https://doi.org/10.1021/es901420b>
- 832 Klompmaker, J. O., Montagne, D. R., Meliefste, K., Hoek, G., & Brunekreef, B. (2015). Spatial
833 variation of ultrafine particles and black carbon in two cities: Results from a short-term
834 measurement campaign. *Science of The Total Environment*, 508, 266–275.
835 <https://doi.org/10.1016/j.scitotenv.2014.11.088>
- 836 Kostenidou, E., Lee, B.-H., Engelhart, G. J., Pierce, J. R., & Pandis, S. N. (2009). Mass Spectra
837 Deconvolution of Low, Medium, and High Volatility Biogenic Secondary Organic
838 Aerosol. *Environmental Science & Technology*, 43(13), 4884–4889.
839 <https://doi.org/10.1021/es803676g>
- 840 Kwon, H.-S., Ryu, M. H., & Carlsten, C. (2020). Ultrafine particles: Unique physicochemical
841 properties relevant to health and disease. *Experimental & Molecular Medicine*, 52(3),
842 Article 3. <https://doi.org/10.1038/s12276-020-0405-1>
- 843 Lalchandani, V., Kumar, V., Tobler, A., M. Thamban, N., Mishra, S., Slowik, J. G., Bhattu, D.,
844 Rai, P., Satish, R., Ganguly, D., Tiwari, S., Rastogi, N., Tiwari, S., Močnik, G., Prévôt,
845 A. S. H., & Tripathi, S. N. (2021). Real-time characterization and source apportionment
846 of fine particulate matter in the Delhi megacity area during late winter. *Science of The
847 Total Environment*, 770, 145324. <https://doi.org/10.1016/j.scitotenv.2021.145324>
- 848 Lanz, V. A., Alfarra, M. R., Baltensperger, U., Buchmann, B., Hueglin, C., & Prévôt, A. S. H.
849 (2007). Source apportionment of submicron organic aerosols at an urban site by factor
850 analytical modelling of aerosol mass spectra. *Atmospheric Chemistry and Physics*, 7(6),
851 1503–1522. <https://doi.org/10.5194/acp-7-1503-2007>



- 852 Lee, B. P., Li, Y. J., Yu, J. Z., Louie, P. K. K., & Chan, C. K. (2015). Characteristics of
853 submicron particulate matter at the urban roadside in downtown Hong Kong—Overview
854 of 4 months of continuous high-resolution aerosol mass spectrometer measurements.
855 *Journal of Geophysical Research: Atmospheres*, *120*(14), 7040–7058.
856 <https://doi.org/10.1002/2015JD023311>
- 857 Lenschow, P., Abraham, H.-J., Kutzner, K., Lutz, M., Preuß, J.-D., & Reichenbacher, W. (2001).
858 Some ideas about the sources of PM₁₀. *Atmospheric Environment*, *35*, S23–S33.
859 [https://doi.org/10.1016/S1352-2310\(01\)00122-4](https://doi.org/10.1016/S1352-2310(01)00122-4)
- 860 Li, Y., Pöschl, U., & Shiraiwa, M. (2016). Molecular corridors and parameterizations of
861 volatility in the chemical evolution of organic aerosols. *Atmospheric Chemistry and
862 Physics*, *16*(5), 3327–3344. <https://doi.org/10.5194/acp-16-3327-2016>
- 863 Li, Z., Fung, J. C. H., & Lau, A. K. H. (2018). High spatiotemporal characterization of on-road
864 PM_{2.5} concentrations in high-density urban areas using mobile monitoring. *Building and
865 Environment*, *143*, 196–205. <https://doi.org/10.1016/j.buildenv.2018.07.014>
- 866 Liu, T., Li, Z., Chan, M., & Chan, C. K. (2017). Formation of secondary organic aerosols from
867 gas-phase emissions of heated cooking oils. *Atmospheric Chemistry and Physics*, *17*(12),
868 7333–7344. <https://doi.org/10.5194/acp-17-7333-2017>
- 869 Liu, T., Wang, Z., Wang, X., & Chan, C. K. (2018). Primary and secondary organic aerosol from
870 heated cooking oil emissions. *Atmospheric Chemistry and Physics*, *18*(15), 11363–11374.
871 <https://doi.org/10.5194/acp-18-11363-2018>
- 872 Louie, P. K. K., Chow, J. C., Chen, L.-W. A., Watson, J. G., Leung, G., & Sin, D. W. M. (2005).
873 PM_{2.5} chemical composition in Hong Kong: Urban and regional variations. *Science of
874 The Total Environment*, *338*(3), 267–281. <https://doi.org/10.1016/j.scitotenv.2004.07.021>



- 875 Louvaris, E. E., Karnezi, E., Kostenidou, E., Kaltsonoudis, C., & Pandis, S. N. (2017).
876 Estimation of the volatility distribution of organic aerosol combining thermodenuder and
877 isothermal dilution measurements. *Atmospheric Measurement Techniques*, 10(10), 3909–
878 3918. <https://doi.org/10.5194/amt-10-3909-2017>
- 879 Marcinkowska, M. A., & Jeleń, H. H. (2022). Role of Sulfur Compounds in Vegetable and
880 Mushroom Aroma. *Molecules*, 27(18), Article 18.
881 <https://doi.org/10.3390/molecules27186116>
- 882 Masoud, C. G., Li, Y., Wang, D. S., Katz, E. F., DeCarlo, P. F., Farmer, D. K., Vance, M. E.,
883 Shiraiwa, M., & Hildebrandt Ruiz, L. (2022). Molecular composition and gas-particle
884 partitioning of indoor cooking aerosol: Insights from a FIGAERO-CIMS and kinetic
885 aerosol modeling. *Aerosol Science and Technology*, 0(0), 1–18.
886 <https://doi.org/10.1080/02786826.2022.2133593>
- 887 Milic, A., Miljevic, B., Alroe, J., Mallet, M., Canonaco, F., Prevot, A. S. H., & Ristovski, Z. D.
888 (2016). The ambient aerosol characterization during the prescribed bushfire season in
889 Brisbane 2013. *Science of The Total Environment*, 560–561, 225–232.
890 <https://doi.org/10.1016/j.scitotenv.2016.04.036>
- 891 Mohr, C., Huffman, J. A., Cubison, M. J., Aiken, A. C., Docherty, K. S., Kimmel, J. R., Ulbrich,
892 I. M., Hannigan, M., & Jimenez, J. L. (2009). Characterization of Primary Organic
893 Aerosol Emissions from Meat Cooking, Trash Burning, and Motor Vehicles with High-
894 Resolution Aerosol Mass Spectrometry and Comparison with Ambient and Chamber
895 Observations. *Environmental Science & Technology*, 43(7), 2443–2449.
896 <https://doi.org/10.1021/es8011518>



- 897 Mohr, C., Richter, R., DeCarlo, P. F., Prévôt, A. S. H., & Baltensperger, U. (2011). Spatial
898 variation of chemical composition and sources of submicron aerosol in Zurich during
899 wintertime using mobile aerosol mass spectrometer data. *Atmospheric Chemistry and*
900 *Physics*, 11(15), 7465–7482. <https://doi.org/10.5194/acp-11-7465-2011>
- 901 Mosqueron, L., Momas, I., & Moullec, Y. L. (2002). Personal exposure of Paris office workers
902 to nitrogen dioxide and fine particles. *Occupational and Environmental Medicine*, 59(8),
903 550–555. <https://doi.org/10.1136/oem.59.8.550>
- 904 N. Pandis, S., Skyllakou, K., Florou, K., Kostenidou, E., Kaltsonoudis, C., Hasa, E., & A. Presto,
905 A. (2016). Urban particulate matter pollution: A tale of five cities. *Faraday Discussions*,
906 189(0), 277–290. <https://doi.org/10.1039/C5FD00212E>
- 907 Omelekhina, Y., Eriksson, A., Canonaco, F., H. Prevot, A. S., Nilsson, P., Isaxon, C., Pagels, J.,
908 & Wierzbicka, A. (2020). Cooking and electronic cigarettes leading to large differences
909 between indoor and outdoor particle composition and concentration measured by aerosol
910 mass spectrometry. *Environmental Science: Processes & Impacts*, 22(6), 1382–1396.
911 <https://doi.org/10.1039/D0EM00061B>
- 912 Raatikainen, T., Vaattovaara, P., Tiitta, P., Miettinen, P., Rautiainen, J., Ehn, M., Kulmala, M.,
913 Laaksonen, A., & Worsnop, D. R. (2010). Physicochemical properties and origin of
914 organic groups detected in boreal forest using an aerosol mass spectrometer. *Atmospheric*
915 *Chemistry and Physics*, 10(4), 2063–2077. <https://doi.org/10.5194/acp-10-2063-2010>
- 916 Renzi, M., Marchetti, S., de' Donato, F., Pappagallo, M., Scortichini, M., Davoli, M., Frova, L.,
917 Michelozzi, P., & Stafoggia, M. (2021). Acute Effects of Particulate Matter on All-Cause
918 Mortality in Urban, Rural, and Suburban Areas, Italy. *International Journal of*



- 919 *Environmental Research and Public Health*, 18(24), Article 24.
- 920 <https://doi.org/10.3390/ijerph182412895>
- 921 Reyes-Villegas, E., Bannan, T., Le Breton, M., Mehra, A., Priestley, M., Percival, C., Coe, H., &
922 Allan, J. D. (2018a). Online Chemical Characterization of Food-Cooking Organic
923 Aerosols: Implications for Source Apportionment. *Environmental Science & Technology*,
924 52(9), 5308–5318. <https://doi.org/10.1021/acs.est.7b06278>
- 925 Reyes-Villegas, E., Bannan, T., Le Breton, M., Mehra, A., Priestley, M., Percival, C., Coe, H., &
926 Allan, J. D. (2018b). Online Chemical Characterization of Food-Cooking Organic
927 Aerosols: Implications for Source Apportionment. *Environmental Science & Technology*,
928 52(9), 5308–5318. <https://doi.org/10.1021/acs.est.7b06278>
- 929 Rogge, W. F., Hildemann, L. M., Mazurek, M. A., Cass, G. R., & Simoneit, B. R. T. (1991a).
930 Sources of fine organic aerosol. 1. Charbroilers and meat cooking operations.
931 *Environmental Science & Technology*, 25(6), 1112–1125.
932 <https://doi.org/10.1021/es00018a015>
- 933 Rogge, W. F., Hildemann, L. M., Mazurek, M. A., Cass, G. R., & Simoneit, B. R. T. (1991b).
934 Sources of fine organic aerosol. 1. Charbroilers and meat cooking operations.
935 *Environmental Science & Technology*, 25(6), 1112–1125.
936 <https://doi.org/10.1021/es00018a015>
- 937 Rose Eilenberg, S., Subramanian, R., Malings, C., Hauryliuk, A., Presto, A. A., & Robinson, A.
938 L. (2020). Using a network of lower-cost monitors to identify the influence of modifiable
939 factors driving spatial patterns in fine particulate matter concentrations in an urban
940 environment. *Journal of Exposure Science & Environmental Epidemiology*, 30(6), Article
941 6. <https://doi.org/10.1038/s41370-020-0255-x>



- 942 Ruggeri, G., & Takahama, S. (2016). Technical Note: Development of chemoinformatic tools to
943 enumerate functional groups in molecules for organic aerosol characterization.
944 *Atmospheric Chemistry and Physics*, 16(7), 4401–4422. [https://doi.org/10.5194/acp-16-](https://doi.org/10.5194/acp-16-4401-2016)
945 4401-2016
- 946 Saha, P. K., Sengupta, S., Adams, P., Robinson, A. L., & Presto, A. A. (2020). Spatial
947 Correlation of Ultrafine Particle Number and Fine Particle Mass at Urban Scales:
948 Implications for Health Assessment. *Environmental Science & Technology*, 54(15),
949 9295–9304. <https://doi.org/10.1021/acs.est.0c02763>
- 950 Saha, P. K., Zimmerman, N., Malings, C., Hauryliuk, A., Li, Z., Snell, L., Subramanian, R.,
951 Lipsky, E., Apte, J. S., Robinson, A. L., & Presto, A. A. (2019). Quantifying high-
952 resolution spatial variations and local source impacts of urban ultrafine particle
953 concentrations. *Science of The Total Environment*, 655, 473–481.
954 <https://doi.org/10.1016/j.scitotenv.2018.11.197>
- 955 Schauer, J. J., Kleeman, M. J., Cass, G. R., & Simoneit, B. R. T. (2002). Measurement of
956 Emissions from Air Pollution Sources. 4. C1–C27 Organic Compounds from Cooking
957 with Seed Oils. *Environmental Science & Technology*, 36(4), 567–575.
958 <https://doi.org/10.1021/es002053m>
- 959 Schauer, J. J., Rogge, W. F., Hildemann, L. M., Mazurek, M. A., Cass, G. R., & Simoneit, B. R.
960 T. (1996). Source apportionment of airborne particulate matter using organic compounds
961 as tracers. *Atmospheric Environment*, 30(22), 3837–3855. [https://doi.org/10.1016/1352-](https://doi.org/10.1016/1352-2310(96)00085-4)
962 2310(96)00085-4
- 963 Schraufnagel, D. E. (2020). The health effects of ultrafine particles. *Experimental & Molecular*
964 *Medicine*, 52(3), Article 3. <https://doi.org/10.1038/s12276-020-0403-3>



- 965 Shah, R. U., Robinson, E. S., Gu, P., Robinson, A. L., Apte, J. S., & Presto, A. A. (2018). High-
966 spatial-resolution mapping and source apportionment of aerosol composition in Oakland,
967 California, using mobile aerosol mass spectrometry. *Atmospheric Chemistry and Physics*,
968 *18*(22), 16325–16344. <https://doi.org/10.5194/acp-18-16325-2018>
- 969 Song, R., Presto, A. A., Saha, P., Zimmerman, N., Ellis, A., & Subramanian, R. (2021a). Spatial
970 variations in urban air pollution: Impacts of diesel bus traffic and restaurant cooking at
971 small scales. *Air Quality, Atmosphere & Health*. [https://doi.org/10.1007/s11869-021-](https://doi.org/10.1007/s11869-021-01078-8)
972 [01078-8](https://doi.org/10.1007/s11869-021-01078-8)
- 973 Song, R., Presto, A. A., Saha, P., Zimmerman, N., Ellis, A., & Subramanian, R. (2021b). Spatial
974 variations in urban air pollution: Impacts of diesel bus traffic and restaurant cooking at
975 small scales. *Air Quality, Atmosphere & Health*, *14*(12), 2059–2072.
976 <https://doi.org/10.1007/s11869-021-01078-8>
- 977 Sturm, P. J., Baltensperger, U., Bacher, M., Lechner, B., Hausberger, S., Heiden, B., Imhof, D.,
978 Weingartner, E., Prevot, A. S. H., Kurtenbach, R., & Wiesen, P. (2003). Roadside
979 measurements of particulate matter size distribution. *Atmospheric Environment*, *37*(37),
980 5273–5281. <https://doi.org/10.1016/j.atmosenv.2003.05.006>
- 981 Sun, Y. L., Wang, Z. F., Fu, P. Q., Yang, T., Jiang, Q., Dong, H. B., Li, J., & Jia, J. J. (2013).
982 Aerosol composition, sources and processes during wintertime in Beijing, China.
983 *Atmospheric Chemistry and Physics*, *13*(9), 4577–4592. [https://doi.org/10.5194/acp-13-](https://doi.org/10.5194/acp-13-4577-2013)
984 [4577-2013](https://doi.org/10.5194/acp-13-4577-2013)
- 985 Sun, Y. L., Zhang, Q., Schwab, J. J., Yang, T., Ng, N. L., & Demerjian, K. L. (2012). Factor
986 analysis of combined organic and inorganic aerosol mass spectra from high resolution



- 987 aerosol mass spectrometer measurements. *Atmospheric Chemistry and Physics*, 12(18),
988 8537–8551. <https://doi.org/10.5194/acp-12-8537-2012>
- 989 Takhar, M., Stroud, C. A., & Chan, A. W. H. (2019). Volatility Distribution and Evaporation
990 Rates of Organic Aerosol from Cooking Oils and their Evolution upon Heterogeneous
991 Oxidation. *ACS Earth and Space Chemistry*, 3(9), 1717–1728.
992 <https://doi.org/10.1021/acsearthspacechem.9b00110>
- 993 Tan, Y., Dallmann, T. R., Robinson, A. L., & Presto, A. A. (2016). Application of plume
994 analysis to build land use regression models from mobile sampling to improve model
995 transferability. *Atmospheric Environment*, 134, 51–60.
996 <https://doi.org/10.1016/j.atmosenv.2016.03.032>
- 997 Torkmahalleh, M. A., Goldasteh, I., Zhao, Y., Udochu, N. M., Rossner, A., Hopke, P. K., &
998 Ferro, A. R. (2012). PM_{2.5} and ultrafine particles emitted during heating of commercial
999 cooking oils. *Indoor Air*, 22(6), 483–491. <https://doi.org/10.1111/j.1600->
1000 0668.2012.00783.x
- 1001 Wallace, L. A., Emmerich, S. J., & Howard-Reed, C. (2004). Source Strengths of Ultrafine and
1002 Fine Particles Due to Cooking with a Gas Stove. *Environmental Science & Technology*,
1003 38(8), 2304–2311. <https://doi.org/10.1021/es0306260>
- 1004 Wan, M.-P., Wu, C.-L., Sze To, G.-N., Chan, T.-C., & Chao, C. Y. H. (2011). Ultrafine particles,
1005 and PM_{2.5} generated from cooking in homes. *Atmospheric Environment*, 45(34), 6141–
1006 6148. <https://doi.org/10.1016/j.atmosenv.2011.08.036>
- 1007 Wang, Y., Bechle, M. J., Kim, S.-Y., Adams, P. J., Pandis, S. N., Pope, C. A., Robinson, A. L.,
1008 Sheppard, L., Szpiro, A. A., & Marshall, J. D. (2020). Spatial decomposition analysis of



- 1009 NO₂ and PM_{2.5} air pollution in the United States. *Atmospheric Environment*, 241,
1010 117470. <https://doi.org/10.1016/j.atmosenv.2020.117470>
- 1011 Wang, Y., Zhu, Y., Salinas, R., Ramirez, D., Karnae, S., & John, K. (2008). Roadside
1012 Measurements of Ultrafine Particles at a Busy Urban Intersection. *Journal of the Air &*
1013 *Waste Management Association*, 58(11), 1449–1457. [https://doi.org/10.3155/1047-](https://doi.org/10.3155/1047-3289.58.11.1449)
1014 3289.58.11.1449
- 1015 Wu, C. L., Chao, C. Y. H., Sze-To, G. N., Wan, M. P., & Chan, T. C. (2012). Ultrafine Particle
1016 Emissions from Cigarette Smouldering, Incense Burning, Vacuum Cleaner Motor
1017 Operation and Cooking. *Indoor and Built Environment*, 21(6), 782–796.
1018 <https://doi.org/10.1177/1420326X11421356>
- 1019 Yao, D., Lyu, X., Lu, H., Zeng, L., Liu, T., Chan, C. K., & Guo, H. (2021). Characteristics,
1020 sources and evolution processes of atmospheric organic aerosols at a roadside site in
1021 Hong Kong. *Atmospheric Environment*, 252, 118298.
1022 <https://doi.org/10.1016/j.atmosenv.2021.118298>
- 1023 Yao, X., Lau, N. T., Fang, M., & Chan, C. K. (2005). Real-Time Observation of the
1024 Transformation of Ultrafine Atmospheric Particle Modes. *Aerosol Science and*
1025 *Technology*, 39(9), 831–841. <https://doi.org/10.1080/02786820500295248>
- 1026 Ye, C., Yuan, B., Lin, Y., Wang, Z., Hu, W., Li, T., Chen, W., Wu, C., Wang, C., Huang, S., Qi,
1027 J., Wang, B., Wang, C., Song, W., Wang, X., Zheng, E., Krechmer, J. E., Ye, P., Zhang,
1028 Z., ... Shao, M. (2021). Chemical characterization of oxygenated organic compounds in
1029 the gas phase and particle phase using iodide CIMS with FIGAERO in urban air.
1030 *Atmospheric Chemistry and Physics*, 21(11), 8455–8478. [https://doi.org/10.5194/acp-21-](https://doi.org/10.5194/acp-21-8455-2021)
1031 8455-2021



- 1032 Zhang, Y., Tang, L., Yu, H., Wang, Z., Sun, Y., Qin, W., Chen, W., Chen, C., Ding, A., Wu, J.,
1033 Ge, S., Chen, C., & Zhou, H. (2015). Chemical composition, sources and evolution
1034 processes of aerosol at an urban site in Yangtze River Delta, China during wintertime.
1035 *Atmospheric Environment*, 123, 339–349.
1036 <https://doi.org/10.1016/j.atmosenv.2015.08.017>
- 1037 Zhang, Z., Zhu, W., Hu, M., Wang, H., Chen, Z., Shen, R., Yu, Y., Tan, R., & Guo, S. (2021).
1038 Secondary Organic Aerosol from Typical Chinese Domestic Cooking Emissions.
1039 *Environmental Science & Technology Letters*, 8(1), 24–31.
1040 <https://doi.org/10.1021/acs.estlett.0c00754>
- 1041 Zhao, H., Chan, W. R., Cohn, S., Delp, W. W., Walker, I. S., & Singer, B. C. (2021). Indoor air
1042 quality in new and renovated low-income apartments with mechanical ventilation and
1043 natural gas cooking in California. *Indoor Air*, 31(3), 717–729.
1044 <https://doi.org/10.1111/ina.12764>
- 1045 Zhao, Y., Hu, M., Slanina, S., & Zhang, Y. (2007a). Chemical Compositions of Fine Particulate
1046 Organic Matter Emitted from Chinese Cooking. *Environmental Science & Technology*,
1047 41(1), 99–105. <https://doi.org/10.1021/es0614518>
- 1048 Zhao, Y., Hu, M., Slanina, S., & Zhang, Y. (2007b). The molecular distribution of fine
1049 particulate organic matter emitted from Western-style fast food cooking. *Atmospheric
1050 Environment*, 41(37), 8163–8171. <https://doi.org/10.1016/j.atmosenv.2007.06.029>
- 1051 Zhu, Q., Huang, X.-F., Cao, L.-M., Wei, L.-T., Zhang, B., He, L.-Y., Elser, M., Canonaco, F.,
1052 Slowik, J. G., Bozzetti, C., El-Haddad, I., & Prévôt, A. S. H. (2018). Improved source
1053 apportionment of organic aerosols in complex urban air pollution using the multilinear

<https://doi.org/10.5194/egusphere-2023-885>

Preprint. Discussion started: 23 May 2023

© Author(s) 2023. CC BY 4.0 License.



1054 engine (ME-2). *Atmospheric Measurement Techniques*, 11(2), 1049–1060.

1055 <https://doi.org/10.5194/amt-11-1049-2018>

1056